Hypoxia-inducible factor promotes cysteine homeostasis in *Caenorhabditis elegans*

Kurt Warnhoff[1,2], Jennifer Snoozy[1], Peter C. Breen[3], and Gary Ruvkun[3]

[1]Pediatrics and Rare Diseases Group, Sanford Research, Sioux Falls, SD 57104, USA
[2]Department of Pediatrics, Sanford School of Medicine, University of South Dakota, Sioux Falls, SD 57105 USA
[3]Department of Molecular Biology, Massachusetts General Hospital, Boston, MA 02114, USA
Correspondence to: Kurt Warnhoff (kurt.warnhoff@sanfordhealth.org)

Abstract:
The amino acid cysteine is critical for many aspects of life, yet excess cysteine is toxic. Therefore, animals require pathways to maintain cysteine homeostasis. In mammals, high cysteine activates cysteine dioxygenase, a key enzyme in cysteine catabolism. The mechanism by which cysteine dioxygenase is regulated remains largely unknown. We discovered that *C. elegans* cysteine dioxygenase (*cdo-1*) is transcriptionally activated by high cysteine and the hypoxia inducible transcription factor (*hif-1*). *hif-1*-dependent activation of *cdo-1* occurs downstream of an H_2S-sensing pathway that includes *rhy-1, cysl-1,* and *egl-9. cdo-1* transcription is primarily activated in the hypodermis where it is sufficient to drive sulfur amino acid metabolism. EGL-9 and HIF-1 are core members of the cellular hypoxia response. However, we demonstrate that the mechanism of HIF-1-mediated induction of *cdo-1* functions largely independent of EGL-9 prolyl hydroxylation and the von Hippel-Lindau E3 ubiquitin ligase; classical hypoxia signaling pathway components. We propose that the intersection of *hif-1* and *cdo-1* reveals a negative feedback loop for maintaining cysteine homeostasis. High cysteine stimulates the production of an H_2S signal. H_2S then activates the *rhy-1/cysl-1/egl-9* signaling pathway, increasing HIF-1-mediated transcription of *cdo-1,* promoting degradation of cysteine via CDO-1.

Introduction:

Cysteine is a sulfur-containing amino acid that mediates many oxidation/reduction reactions of proteins, is a substrate in the production of iron-sulfur clusters and hydrogen sulfide (H_2S), a volatile signaling molecule, and a precursor to the antioxidant glutathione (1-3). Cysteine residues in close proximity in the primary or folded protein sequence are oxidized in the endoplasmic reticulum to form intra- and interprotein disulfide linkages, most commonly in secreted proteins which mediate intercellular signaling and defense (4-6). In many enzymes, the reactivity of the cysteine sulfur is key for the coordination of metals such as zinc or iron, which support protein structure and catalytic activity (7-9). In contrast to its essential function, excess cysteine is also toxic. High cysteine impairs mitochondrial respiration by disrupting iron homeostasis (10), acts as a neural excitotoxin (11), and promotes the formation of toxic levels of hydrogen sulfide gas (2, 12, 13). Given this balance between essential and toxic, cysteine homeostasis is key for the health of cells and organisms.

Cysteine is oxidized to cysteinesulfinate by cysteine dioxygenase (CDO-1 in *C. elegans,* CDO1 in mammals) (**Fig. 1A)** (14)**.** CDO1-mediated oxidation is the primary pathway of cysteine catabolism when sulfur amino acid (methionine or cysteine) availability is normal or high (15). As a critical player in cysteine homeostasis, CDO1 is a highly regulated enzyme: the activity and abundance of CDO1 increase dramatically in cells and animals fed excess cysteine and methionine (16). CDO1 activation is governed both transcriptionally and post-translationally via the 26S proteasome (17-21). However, the molecular players that sense high cysteine and promote CDO1 activation remain incompletely defined.

CDO1 dysfunction is also implicated in disease. CDO1 is a tumor suppressor whose activity is silenced in diverse cancers via promoter methylation, a potential biomarker of tumor grade and progression (22-24). Decreased CDO1 activity may support tumor cell growth by reducing reactive oxygen species and decreasing drug susceptibility (25-28).

Using the nematode *C. elegans,* we have shown that CDO-1 is a key player in the pathophysiology of 2 fatal inborn errors of metabolism; molybdenum cofactor deficiency (MoCD) and isolated sulfite oxidase deficiency (ISOD) (29, 30). Molybdenum cofactor (Moco) is an essential 520 Dalton prosthetic group synthesized from GTP by a conserved multistep biosynthetic pathway that is present in about 2/3 of bacterial genomes and nearly all eukaryotic genomes (31, 32). *C. elegans* can either retrieve Moco synthesized by the bacteria it consumes or can synthesize Moco *de novo* using its own Moco biosynthetic pathway (33). *C. elegans* strains carrying mutations in genes encoding Moco biosynthetic enzymes (*moc*) and feeding on wild-type *E. coli* develop normally. Yet, these same *moc*-mutant *C. elegans* fed Moco-deficient *E. coli* are completely inviable. A genetic selection for mutations that suppress this inviability identified mutations in *cth-2* (cystathionase) and *cdo-1* (cysteine dioxygenase), enzymes in the cysteine biosynthetic and degradation pathway. Using the dipeptide cystathionine as a substrate, CTH-2 produces α-ketobutyrate and cysteine. Cysteine is further oxidized by CDO-1, generating highly toxic sulfites. These sulfites are normally oxidized to more benign sulfate by Moco-requiring sulfite oxidase, SUOX-1, an essential enzyme in *C. elegans* and humans (**Fig. 1A**) (30, 33). Therefore, loss of *cdo-1* or *cth-2* suppresses the lethality caused by Moco deficiency in *C. elegans* by not producing sulfites which are toxic when SUOX-1 is inactive due to Moco deficiency (33-35). Thus, understanding the fundamental mechanisms that govern the levels and activity of CDO-1 is critical to generating new therapeutic hypotheses to treat these diseases.

To define genes that regulate *cdo-1* levels and activity, we performed an unbiased genetic screen in the nematode *C. elegans* to identify mutations that increase the expression or abundance of CDO-1. We identified loss-of-function mutations in 2 genes, *egl-9* and *rhy-1*, that dramatically increase expression of a P*cdo-1::CDO-1::GFP* reporter transgene. These enzymes act in the hypoxia and H_2S-sensing pathway, and we demonstrate that the conserved hypoxia-inducible transcription factor (HIF-1) activates *cdo-1* transcription in this pathway (36-38). We further show that high cysteine promotes *cdo-1* transcription, and that *hif-1* and *cysl-1* (another component of the H_2S-sensing pathway) are required for viability under high cysteine conditions. We demonstrate that transcriptional activation of *cdo-1* via HIF-1 promotes CDO-1 activity and establish the *C. elegans* hypodermis as a key tissue of CDO-1 activation and function. Unexpectedly, we find that *cdo-1*

regulation is governed by a HIF-1 pathway largely independent of EGL-9 prolyl hydroxylase activity and von Hippel-Lindau (VHL-1), the canonical oxygen-sensing pathway (39, 40). These data establish a new connection between the HIF-1/H_2S-sensing pathway and sulfur amino acid catabolism governed by CDO-1.

Results:

egl-9 and *rhy-1* negatively regulate *cdo-1* transcription:

To identify regulators of CDO-1 levels, we engineered a transgene expressing a C-terminal green fluorescent protein (GFP) tagged version of full-length CDO-1 protein driven by the native *cdo-1* promoter (*Pcdo-1::CDO-1::GFP*, **Fig. 1B**). Transgenic animals were generated by integrating the *Pcdo-1::CDO-1::GFP* construct into the *C. elegans* genome (41). This transgene was functional and rescued a *cdo-1* loss of function mutation (**Fig. S1**). The *Pcdo-1::CDO-1::GFP* transgene reverses the suppression of Moco-deficient lethality caused by *cdo-1* loss of function (**Fig. S1**). The reanimation of Moco-deficient lethality by the transgene depends on CDO-1 enzymatic activity because a transgene expressing an active-site mutant *Pcdo-1::CDO-1[C85Y]::GFP* does not rescue the *cdo-1* mutant phenotype (**Fig. S1**) (33, 42). These data demonstrate that the *Pcdo-1::CDO-1::GFP* reporter transgene is functional and suggests its expression pattern reflects endogenous protein expression, localization, and levels.

We performed a mutagenesis screen to identify genes that control the expression or accumulation of CDO-1 protein. Specifically, we performed an EMS chemical mutagenesis of *C. elegans* and screened for mutations that caused increased GFP accumulation by the *Pcdo-1::CDO-1::GFP* reporter transgene. New mutants were isolated two generations post mutagenesis to allow novel mutations to become homozygous (43). Using whole-genome sequencing, we determined that 2 independently isolated mutants carried distinct mutations in *egl-9* and four other independently isolated mutants had unique mutations in *rhy-1* (**Fig. 1C)**. The presence of multiple independent alleles suggests these mutations in *egl-9* or *rhy-1* are causative for the increased *Pcdo-1::CDO-1::GFP* expression or accumulation phenotype. *egl-9* encodes the oxygen-sensing prolyl hydroxylase and orthologue of mammalian EGLN1. *rhy-1* encodes the regulator of hypoxia inducible transcription factor, an enzyme with homology to membrane-bound O-acyltransferases (36, 39). The genetic screen produced nonsense alleles of both *egl-9* and *rhy-1* suggesting the increased *Pcdo-1::CDO-1::GFP* expression or accumulation phenotype is caused by loss of *egl-9* or *rhy-1* function (**Fig. 1C**). Inactivation of *egl-9* or *rhy-1* activates a transcriptional program mediated by the hypoxia inducible transcription factor, HIF-1 (36, 39). To determine if *egl-9* or *rhy-1* regulate *cdo-1* transcription, we engineered a separate reporter construct where only GFP is transcribed by the *cdo-1* promoter (*Pcdo-1::GFP,* **Fig. 1B**). This *Pcdo-1::GFP* transgene was introduced into strains with independently isolated *egl-9(sa307)* and *rhy-1(ok1402)* null reference alleles (36, 44). The *egl-9(sa307)* and *rhy-1(ok1402)* mutations dramatically induce GFP driven by the *Pcdo-1::GFP* transgene (**Fig. 1D,E**). The activation of *cdo-1* transcription by independently isolated *egl-9* or *rhy-1* mutations demonstrates that the *egl-9* and *rhy-1* mutations isolated in our screen for the induction or accumulation of *Pcdo-1::CDO-1::GFP* are the causative genetic lesions. Furthermore, these data demonstrate that *egl-9* and *rhy-1* are necessary for the normal transcriptional repression of *cdo-1.*

HIF-1 directly activates *cdo-1* transcription downstream of the *rhy-1, cysl-1, egl-9* genetic pathway:

rhy-1 and *egl-9* act in a pathway that regulates the abundance and activity of the HIF-1 transcription factor (36, 38). The activity of *rhy-1* is most upstream in the pathway and negatively regulates the activity of *cysl-1,* which encodes a cysteine synthase-like enzyme likely of algal origin (45). CYSL-1 directly binds to and inhibits EGL-9 in an H_2S-modulated manner (38). EGL-9 uses molecular oxygen as well as an α-ketoglutarate cofactor to directly inhibit HIF-1 via prolyl hydroxylation, which recruits the VHL-1 ubiquitin ligase to ubiquitinate HIF-1, targeting it for degradation by the proteasome (46-48). Given that loss-of-function mutations in *rhy-1* or *egl-9* activate *cdo-1* transcription, we tested if *cdo-1* transcription is activated by HIF-1 as an output of this hypoxia/H_2S-sensing pathway. We performed epistasis studies using null mutations that inhibit the activity of *hif-1* (*cysl-1(ok762)* and *hif-1(ia4)*) or activate *hif-1* (*rhy-1(ok1402)* and *egl-9(sa307)*). The induction of *Pcdo-1::GFP* by *egl-9* inactivation was dependent upon the activity of *hif-1,* but not on the activity of *cysl-1* (**Fig. 2A,B)**. In contrast, induction of *Pcdo-1::GFP* by *rhy-1* inactivation was dependent upon the activity of both *hif-1* and *cysl-1* (**Fig. 2A,C)**. These results reveal a genetic pathway whereby *rhy-1, cysl-1,* and *egl-9* function in a negative-regulatory cascade to control the activity of HIF-1 which transcriptionally activates *cdo-1.* Our epistasis studies of *cdo-1* transcriptional regulation by HIF-1 align well with previous analyses of this genetic pathway in the context of transcription of *cysl-2* (a paralog of *cysl-1*) and the "O_2-ON response" (38).

To demonstrate that HIF-1 activates transcription of endogenous *cdo-1,* we explored published RNA-sequencing data of wild-type, *egl-9(-),* and *egl-9(-) hif-1(-)* mutant animals (49). *egl-9(-)* mutant *C. elegans* display an 8-fold increase in *cdo-1* mRNA compared to wild type. This induction was dependent on *hif-1;* a *hif-1(-)* mutation completely suppressed the induction of *cdo-1* mRNA caused by an *egl-9(-)* mutation (49). These RNA-seq data confirm our findings using the *Pcdo-1::GFP* transcriptional reporter that HIF-1 is a transcriptional activator of *cdo-1.* ChIP-seq data of HIF-1 performed by the modERN project show that HIF-1 directly binds the *cdo-1* promoter (peak from -1,165 to -714 base pairs 5' to the *cdo-1* ATG start codon) (50). This HIF-1 binding site contains 3 copies of the HIF-binding motif (5'-RCGTG-3') (51). We conclude that *cdo-1* is a downstream effector of HIF-1 and is likely a direct transcriptional target of HIF-1.

High cysteine promotes *cdo-1* transcription and *cysl-1* and *hif-1* are necessary for survival on high cysteine:

Mammalian CDO1 levels and activity are highly induced by dietary cysteine (14-16). To determine if this homeostatic response is conserved in *C. elegans,* we exposed transgenic *C. elegans* carrying the *Pcdo-1::GFP* transcriptional reporter to high supplemental cysteine (100μM). Like our *egl-9* and *rhy-1* loss-of-function mutations, high cysteine promoted *cdo-1* transcription (**Fig. 3**).

We hypothesized that cysteine might activate *cdo-1* transcription through the RHY-1/CYSL-1/EGL-9/HIF-1 pathway. In this pathway, *cysl-1* and *hif-1* act to promote *cdo-1* transcription. We tested whether *cysl-1* or *hif-1* were necessary for the induction of *Pcdo-1::GFP* by high cysteine. However, this experiment was not possible as we observed 100% lethality in *cysl-1(-); Pcdo-1::GFP* (*n*=174 individuals) and *hif-1(-); Pcdo-1::GFP* (*n*=139 individuals) animals when exposed to 100μM supplemental cysteine. In contrast, 100% of *cysl-1(-); Pcdo-1::GFP* (*n*=143 individuals) and 99% *hif-1(-); Pcdo-1::GFP* (n=110 individuals) animals were alive under

control conditions without supplemental cysteine. Wild-type *C. elegans* carrying the *Pcdo-1::GFP* reporter transgene were healthy under control (100% alive, *n*=134 individuals) and high-cysteine (100% alive, *n*=140 individuals) conditions. These data demonstrate that *cysl-1* and *hif-1* are necessary for survival under high cysteine conditions.

Given the established role of CDO-1 in cysteine catabolism, we tested whether *cdo-1(-)* mutants were also sensitive to high cysteine. 98% of *cdo-1(-)* mutants were alive after exposure to 100μM supplemental cysteine (*n*=141 individuals). 100% of *cdo-1(-)* mutant animals were alive in the control group not exposed to high cysteine (*n*=142 individuals). Similarly, wild-type *C. elegans* were healthy under control (100% alive, *n*=131 individuals) and high-cysteine (100% alive, *n*=153 individuals) conditions. Thus, *cdo-1* is not necessary for survival under high cysteine conditions. This suggests the existence of alternate pathways that promote cysteine homeostasis. Given the requirement of *cysl-1* and *hif-1* for survival in high cysteine, we propose that HIF-1 activates pathways (in addition to *cdo-1*) that promote survival under high cysteine conditions.

Activated CDO-1 accumulates and is functional in the hypodermis:

We sought to identify the site of action of CDO-1. To observe CDO-1 localization, we used CRISPR/Cas9 to insert the GFP open reading frame into the endogenous *cdo-1* locus, fused in place of the native *cdo-1* stop codon. This new *cdo-1(rae273)* allele encodes a C-terminal tagged "CDO-1::GFP" protein from the native *cdo-1* genomic locus (**Fig. 4A**). To determine if CDO-1::GFP was functional, we combined CDO-1::GFP with a loss-of-function mutation in *moc-1,* a gene that is essential for *C. elegans* Moco biosynthesis (33). We then observed the growth of *moc-1(-)* CDO-1::GFP *C. elegans* on wild-type and Moco-deficient *E. coli. moc-1(-)* mutant *C. elegans* expressing CDO-1::GFP from the native *cdo-1* locus arrest during larval development when fed Moco-deficient *E. coli,* but not when fed Moco-producing *E.coli* (**Fig. 4C**). This lethality is caused by the CDO-1-mediated production of sulfites which are only toxic when *C. elegans* is Moco deficient, and demonstrates that the CDO-1::GFP fusion protein is functional (33). These data suggest that the CDO-1::GFP expression we observe is physiologically relevant.

When wild-type animals expressing CDO-1::GFP were grown under standard culture conditions, we observed CDO-1::GFP expression in multiple tissues including prominent expression in the hypodermis (**Fig. 4B, Fig. S2**). We tested if CDO-1::GFP levels would be affected by inactivation of *egl-9* or *rhy-1.* We generated *egl-9(-);* CDO-1::GFP and *rhy-1(-);* CDO-1::GFP animals and assayed expression of CDO-1::GFP. Consistent with our studies using *Pcdo-1::CDO-1::GFP* and *Pcdo-1::GFP* transgenes, we found that CDO-1::GFP levels, encoded by *cdo-1(rae273),* were increased by *egl-9(-)* or *rhy-1(-)* mutations (**Fig. 4B, Fig. S2**). Furthermore, high cysteine also promoted accumulation of CDO-1::GFP (**Fig. S3**). In all scenarios, the hypodermis was the most prominent site of CDO-1::GFP accumulation. Specifically, we found that CDO-1::GFP was expressed in the cytoplasm of Hyp7, the major *C. elegans* hypodermal cell (**Fig. 4B**).

Based on the expression pattern of CDO-1::GFP encoded by *cdo-1(rae273)*, we hypothesized that CDO-1 acts in the hypodermis to promote sulfur amino acid metabolism. To test this hypothesis, we engineered a *cdo-1* rescue construct in which *cdo-1* is expressed exclusively in the hypodermis under the control of the *col-10* promoter (*Pcol-10::CDO-1::GFP*) (52). Multiple independent transgenic *C. elegans* strains

were generated by integrating the *Pcol-10::CDO-1::GFP* construct into the *C. elegans* genome (41). We tested the ability of the *Pcol-10::CDO-1::GFP* transgene to rescue the *cdo-1(-)* mutant suppression of Moco-deficient larval arrest. We found that multiple independent transgenic strains of *cdo-1(-) moc-1(-)* double mutant animals carrying the *Pcol-10::CDO-1::GFP* transgene displayed a larval arrest phenotype when fed a Moco-deficient diet (**Fig. 4D**). These data demonstrated that hypodermal-specific expression of *cdo-1* is sufficient to rescue the *cdo-1(-)* mutant suppression of Moco-deficient lethality. This rescue was dependent upon the enzymatic activity of CDO-1 as an active site variant of this transgene (*Pcol-10::CDO-1[C85Y]::GFP)* did not rescue the suppressed larval arrest of *cdo-1(-) moc-1(-)* double mutant animals fed Moco-deficient diets (**Fig. 4D**). Taken together, our analyses of CDO-1::GFP expression demonstrate that CDO-1 is expressed, and that expression is regulated, in multiple tissues, principal among them being the hypodermis and Hyp7 cell. Our tissue-specific rescue data demonstrate that hypodermal expression of *cdo-1* is sufficient to promote cysteine catabolism and suggest that the hypodermis is a critical tissue for sulfur amino acid metabolism. However, we cannot exclude the possibility that CDO-1 also acts in other cells and tissues.

HIF-1 promotes CDO-1 activity downstream of the H_2S-sensing pathway:

We sought to determine the physiological impact of *cdo-1* transcriptional activation by HIF-1. We reasoned mutations that activate HIF-1 and increase *cdo-1* transcription may cause increased CDO-1 activity. CDO-1 sits at a critical metabolic node in the degradation of the sulfur amino acids cysteine and methionine (**Fig 1A**). A key byproduct of sulfur amino acid metabolism and CDO-1 is sulfite, a reactive toxin that is detoxified by the Moco-requiring sulfite oxidase (SUOX-1). Null mutations in *suox-1* cause larval lethality. However, animals carrying the *suox-1(gk738847)* hypomorphic allele are healthy under standard culture conditions (33, 34). *suox-1(gk738847)* mutant animals display only 4% SUOX-1 activity compared to wild type, and are exquisitely sensitive to sulfite stress (53). Thus, the *suox-1(gk738847)* mutation creates a sensitized genetic background to probe for increases in endogenous sulfite production. To test if increased *cdo-1* transcription would impact the growth of *suox-1*-comprimised animals, we combined the *egl-9* null mutation, which promotes HIF-1 activity and *cdo-1* transcription, with the *suox-1(gk738847)* allele. While *egl-9(-)* and *suox-1(gk738847)* single mutant animals are healthy under standard culture conditions, the *egl-9(-); suox-1(gk738847)* double mutant animals are extremely sick and slow growing, establishing a synthetic genetic interaction between these loci (**Table 1**). To determine the role of sulfur amino acid metabolism in the *egl-9(-); suox-1(gk738847)* synthetic sick/slow growth phenotype, we engineered *egl-9(-); cdo-1(-) suox-1(gk738847)* and *cth-2(-); egl-9(-); suox-1(gk738847)* triple mutant animals. The *egl-9; suox-1* synthetic sick/slow growth phenotype was suppressed by inactivating mutations in *cdo-1* or *cth-2* which block the endogenous production of sulfite (**Table 1**). These data demonstrate that the deleterious activity of the *egl-9(-)* mutation in a *suox-1(gk738847)* background requires functional sulfur amino acid metabolism.

To determine the role of the H_2S-sensing pathway in the synthetic sick/slow growth phenotype displayed by *egl-9(-); suox-1(gk738847)* double mutant animals, we introduced null alleles of *cysl-1* or *hif-1* into the *egl-9(-); suox-1(gk738847)* double mutant. The *egl-9; suox-1* synthetic sick/slow growth phenotype was dependent upon *hif-1* but not *cysl-1* (**Table 1**). These results are consistent with our proposed genetic pathway

and support the model that transcriptional activation of *cdo-1* by HIF-1 causes increased CDO-1 activity and increased flux of sulfur amino acids through their catabolic pathway.

Loss of *rhy-1* also strongly activates *cdo-1* transcription. We hypothesized that *rhy-1(-); suox-1(gk738847)* double mutant animals would display a synthetic sick/slow growth phenotype like *egl-9(-); suox-1(gk738847)* double mutant animals. However, *rhy-1(-); suox-1(gk738847)* double mutant animals were just as healthy as either *rhy-1(-)* or *suox-1(gk738847)* single mutant *C. elegans* (**Table 1**). These data suggest that increasing *cdo-1* transcription alone is not sufficient to promote sulfite production via CDO-1. In addition to the role played by *rhy-1* in the regulation of HIF-1 activity, *rhy-1* itself is a transcriptional target of HIF-1. Loss of *egl-9* activity induces *rhy-1* mRNA ~50-fold in a *hif-1*-dependent manner (49). Given this potent transcriptional activation, we wondered if *rhy-1* might play an additional role downstream of HIF-1 in the regulation of sulfur amino acid metabolism and sulfite production. To test this hypothesis, we engineered *rhy-1(-); egl-9(-); suox-1(gk738847)* triple mutant animals. To our surprise, the *rhy-1(-); egl-9(-); suox-1(gk738847)* triple mutant animals were healthy, demonstrating that *rhy-1* was necessary for the deleterious activity of the *egl-9(-)* mutation in a *suox-1(gk738847)* background. These genetic data suggest a dual role for *rhy-1* in the control of sulfur amino acid metabolism; first as a component of a regulatory cascade that controls the activity of HIF-1 and second as a functional downstream effector of HIF-1 that is required for sulfur amino acid metabolism.

This is not the first description of a *rhy-1* role downstream of *hif-1.* Overexpression of a *rhy-1*-encoding transgene suppresses the lethality of a *hif-1(-)* mutant during H_SS stress (54). These data establish RHY-1 as both a regulator and effector of HIF-1. How RHY-1, a predicted membrane-bound O-acyltransferase, molecularly executes these dual roles remains to be explored.

EGL-9 prolyl hydroxylase activity and VHL-1 are largely dispensable in the regulation of CDO-1:

EGL-9 inhibits HIF-1 through its prolyl hydroxylase domain (PHD) (**Fig. 5A**) (39). To evaluate the impact of the EGL-9 PHD on the regulation of *cdo-1*, we generated a PHD-inactive *egl-9* mutation using CRISPR/Cas9. We engineered an *egl-9* mutation that substitutes an alanine in place of histidine 487 (H487A) (**Fig. 1C**). Histidine 487 of EGL-9 is highly conserved and catalytically essential in the PHD active site (**Fig. 5B**) (55, 56). To evaluate the impact of an inactive EGL-9 PHD on the transcription of *cdo-1,* we engineered a *C. elegans* strain carrying the *egl-9(H487A)* mutation with the *Pcdo-1::GFP* transcriptional reporter. *egl-9(H487A)* caused a modest increase in *Pcdo-1::GFP* accumulation in the *C. elegans* intestine, suggesting that the EGL-9 PHD is necessary to repress *cdo-1* transcription in the intestine (**Fig. 5C,D**). However, the activation of *Pcdo-1::GFP* by the *egl-9(H487A)* mutation was markedly less when compared to *Pcdo-1::GFP* activation caused by an *egl-9(-)* null mutation (**Fig. 5C,D**). These data suggest that EGL-9 has a PHD-independent activity that is responsible for repressing *cdo-1* transcription.

EGL-9 PHD hydroxylates specific proline residues on HIF-1. These hydroxylated proline residues are recognized by the von Hippel-Lindau E3 ubiquitin ligase (VHL-1). VHL-1-mediated ubiquitination promotes degradation of HIF-1 by the proteasome (**Fig. 5A**) (40). Thus, the EGL-9 PHD and VHL-1 act in a pathway to regulate HIF-1. To determine the role of VHL-1 in regulating *cdo-1,* we engineered a *C. elegans* strain carrying the *vhl-1(-)* null mutation with our P*cdo-1::GFP* reporter. *vhl-1* inactivation also caused a modest increase in

Pcdo-1::GFP expression in the *C. elegans* intestine, suggesting that *vhl-1* is necessary to repress *cdo-1* transcription (**Fig. 5C,D**). However, activation of *Pcdo-1::GFP* by the *vhl-1(-)* mutation was less than activation caused by an *egl-9(-)* null mutation (**Fig. 5C,D**). These data suggest that EGL-9 has a VHL-1-independent activity that is responsible for repressing *cdo-1* transcription.

To evaluate the impact of inactivating the EGL-9 PHD or VHL-1 on cysteine metabolism, we again employed the *suox-1(gk738847)* hypomorphic mutation that sensitizes animals to increases in sulfite. We engineered *egl-9(H487A); suox-1(gk738847)* and *vhl-1(-) suox-1(gk738847)* double mutant animals and evaluated the health of those strains. In contrast to *egl-9(-); suox-1(gk738847)* double mutant animals which are extremely sick/slow growing, *egl-9(H487A); suox-1(gk738847)* and *vhl-1(-) suox-1(gk738847)* double mutant animals are healthy (**Table 1**). These genetic data suggest that neither the EGL-9 PHD nor VHL-1 are necessary to repress cysteine catabolism/sulfite production. However, it is plausible that the *egl-9(H487)* or *vhl-1(-)* mutations modestly activate cysteine metabolism, likely proportional to their activation of the *Pcdo-1::GFP* transgene (**Fig. 5C,D**), and that this activation is not sufficient to produce enough sulfites to negatively impact the growth of *suox-1(gk738847)* mutant animals.

Discussion:

CDO-1 is a physiologically relevant effector of HIF-1:

The hypoxia-inducible factor HIF-1 is a master regulator of the cellular response to hypoxia. It activates the transcription of many genes and pathways that are critical to maintain metabolic homeostasis in the face of low oxygen. For example, mammalian HIF1A induces the hematopoietic growth hormone erythropoietin, glucose transport and glycolysis, as well as lactate dehydrogenase (57-60). The nematode *C. elegans* encounters a range of oxygen tensions in its natural habitat of rotting material: as microbial abundance increases, oxygen levels decrease from atmospheric levels (~21% O_2). In fact, *C. elegans* prefers 5-12% O_2, perhaps because hypoxia predicts abundant bacterial food sources (61). Elements of the HIF-1 pathway have emerged from *C. elegans* genetics as have critical targets of HIF-1 (39). For instance, *C. elegans* HIF-1 promotes H_2S homeostasis by inducing transcription of the mitochondrial sulfide quinone oxidoreductase (*sqrd-1),* detoxifying H_2S (37).

We sought to define genes that regulate the levels and activity of cysteine dioxygenase (CDO-1), a critical regulator of cysteine homeostasis (14-16). Taking an unbiased genetic approach in *C. elegans,* we found that *cdo-1* was highly regulated by HIF-1 downstream of a signaling pathway that includes *rhy-1*, *cysl-1*, and *egl-9*. We demonstrated that HIF-1 promotes *cdo-1* transcription, accumulation of CDO-1 protein, and increased CDO-1 activity. Loss of *rhy-1* or *egl-9* activate *hif-1* to in turn strongly induce the *cdo-1* promoter. The pathway for activation of *cdo-1* also requires *cysl-1,* which functions downstream of *rhy-1* and upstream of *egl-9.* Based on ChIP-Seq studies, HIF-1 directly binds to the *cdo-1* promoter (50).

We also show that the transcriptional activation of *cdo-1* by HIF-1 promotes CDO-1 enzymatic activity. Genetic activation of *cdo-1* by loss of *egl-9* causes severe sickness in a mutant with reduced sulfite oxidase activity, an activity required to cope with the toxic products of CDO-1. This synthetic sickness is dependent

upon an intact HIF-1 signaling pathway and a functioning sulfur amino acid metabolism pathway, as the dramatic sickness of an *egl-9; suox-1* double mutant is suppressed by loss of *hif-1, cth-2,* or *cdo-1.* These striking genetic results validate the intersection of HIF-1 and CDO-1 as converging biological regulatory pathways and encourage further exploration of this regulatory node. The potential physiological relevance of the connection between HIF-1 signaling and cysteine metabolism is discussed below.

Evidence for distinct pathways of HIF-1 activation by hypoxia and cysteine/H_2S:

The hypoxia-signaling pathway is defined by EGL-9-dependent prolyl hydroxylation of HIF-1. Hydroxylated HIF-1 is then targeted for degradation via VHL-1-mediated ubiquitination (39, 40, 51). However, multiple lines of evidence, reinforced by our work, demonstrate VHL-1- and prolyl hydroxylase-independent activity of EGL-9. *egl-9(-)* null mutant *C. elegans* accumulate HIF-1 protein and display increased transcription of many genes, including *nhr-57,* an established target of HIF-1 (36). In rescue experiments of an *egl-9(-)* null mutant, Shao *et al.* (2009) demonstrate that a wild-type *egl-9* transgene restores normal HIF-1 protein levels and HIF-1 transcription. However, rescue experiments with a PHD-inactive *egl-9(H487A)* transgene do not correct the accumulation of HIF-1 protein and only partially reduce the HIF-1 transcriptional output (56). Through our studies of *cdo-1* transcription, we demonstrate that an *egl-9(H487A)* mutant incompletely activates HIF-1 transcription when compared to an *egl-9(-)* null mutation (**Fig. 5C,D).** Taken together, we conclude EGL-9 has activity independent of its PHD domain, mirroring and supporting previous work (56).

In studies of the HIF-1-dependent P*nhr-57::GFP* transcriptional reporter, Shen *et al.* (2006) observed that *egl-9(-)* null mutants promote HIF-1 transcription more than a *vhl-1(-)* mutant (36). We observe this same distinction between *egl-9* and *vhl-1* mutations with our *Pcdo-1::GFP* reporter (**Fig. 5C,D).** This difference in transcriptional activity is not explained by HIF-1 protein levels as HIF-1 protein accumulated equally in *egl-9(-)* and *vhl-1(-)* null mutants (36). This observation suggests that EGL-9 represses both HIF-1 levels and activity. This study also notes that *vhl-1* represses HIF-1 transcription in the intestine while *egl-9* acts in a wider array of tissues including the intestine and the hypodermis (36). Budde and Roth (2010) also demonstrate that loss of *vhl-1* promotes HIF-1 transcription in the *C. elegans* intestine while total loss of *egl-9* promotes HIF-1 transcription in multiple tissues including the intestine and the hypodermis (62). Our data expand upon these observations by demonstrating that loss of the EGL-9 PHD promotes *cdo-1* transcription in the intestine alone, mirroring the loss of *vhl-1* **(Fig. 5C**). Budde and Roth (2010) additionally demonstrate that physiologically relevant stimuli also elicit a tissue-specific transcriptional response: hypoxia promotes HIF-1 transcription in the intestine while H_2S promotes HIF-1 transcription in the hypodermis. Importantly, H_2S promotes hypodermal HIF-1 transcription in a *vhl-1(-)* mutant, demonstrating a VHL-1-independent pathway for H_2S activation of HIF-1 (62). We demonstrate that high cysteine promotes *cdo-1* transcription in the hypodermis. Taken together with our data, these studies suggest 2 distinct pathways for activating HIF-1 transcription: i) a hypoxia-sensing pathway that is dependent upon *vhl-1* and the EGL-9 PHD and promotes HIF-1 activity in the intestine and ii) an H_2S-sensing pathway that is independent of *vhl-1* and the EGL-9 PHD and promotes HIF-1 activity in the hypodermis.

The genetic details of the H_2S-sensing pathway were solidified through studies of *rhy-1* in *C. elegans.* Ma *et al.* (2012) demonstrate that *hif-1* repression via *rhy-1* requires the activity of *cysl-1,* a gene encoding a cysteine synthase-like protein (38). They further demonstrate that high H_2S promotes a physical interaction between CYSL-1 and EGL-9, resulting in the inactivation of EGL-9 and increased HIF-1 activity. Together, these studies suggest distinct genetic regulators of EGL-9/HIF-1 signaling: *rhy-1* and *cysl-1* govern the H_2S-sensing pathway while *vhl-1* mediates the hypoxia-sensing pathway. These pathways are distinct in their requirement for the EGL-9 PHD.

A negative feedback loop senses high cysteine/H_2S, promotes CDO-1 activity, and maintains cysteine homeostasis:

Why would the RHY-1/CYSL-1/EGL-9/HIF-1 H_2S-sensing pathway control the levels and activity of cysteine dioxygenase? We speculate this intersection facilitates a homeostatic pathway allowing *C. elegans* to sense and respond to cysteine level. We propose that H_2S acts as a gaseous signaling molecule to promote cysteine catabolism. H_2S activates HIF-1 in the hypodermis by promoting the CYSL-1-mediated inactivation of EGL-9 (38). We show that high cysteine similarly induces *cdo-1* transcription in the hypodermis. Our genetic data demonstrate that *cdo-1* is induced by the same genetic pathway that senses H_2S in *C. elegans* and CDO-1 acts in the hypodermis, the major site of H_2S-induced transcription. Furthermore, H_2S induces endogenous *cdo-1* transcription >3-fold but *cdo-1* mRNA levels do not change when *C. elegans* are exposed to hypoxia (63, 64). Thus, it is likely that H_2S promotes *cdo-1* transcription through RHY-1, CYSL-1, EGL-9, and HIF-1. H_2S is a reasonable small molecule signal to alert cells to high cysteine stress. Excess cysteine results in the production of H_2S mediated by multiple enzymes including cystathionase (CTH), cystathionine β-synthase (CBS), and 3-mercaptopyruvate sulfurtransferase (MST) (2, 65). We speculate that excess cysteine in *C. elegans* promotes the enzymatic production of H_2S which would activate HIF-1 via the RHY-1/CYSL-1/EGL-9 signaling pathway. In this homeostatic model, H_2S-activated HIF-1 would then induce *cdo-1* transcription, promoting CDO-1 activity and the catabolism of the high-cysteine trigger (**Fig. 6**). Supporting this model, *cysl-1(-)* and *hif-1(-)* mutant *C. elegans* cannot survive in a high cysteine environment, demonstrating their central role in promoting cysteine homeostasis.

Members of the H_2S-sensing pathway have also been implicated in the *C. elegans* response to infection (44, 66). Many secreted proteins that mediate intercellular signaling or innate immune responses to pathogens are cysteine-rich and form disulfide bonds in the endoplasmic reticulum before protein secretion (67, 68). Levels of free cysteine may fall during the massive inductions of cysteine-rich secreted proteins in development or immune defense (69). The oxidation of so many cysteines to disulfides in the endoplasmic reticulum might locally lower oxygen levels preventing EGLN1 hydroxylation of HIF1A. Thus, the intersection between oxygen sensing and cysteine homeostasis we have uncovered may contribute to a regulatory axis in cell-cell signaling during development and in immune function.

Methods:

General methods and strains:

C. elegans were cultured using established protocols (43). Briefly, animals were cultured at 20°C on nematode growth media (NGM) seeded with wild-type *E. coli* (OP50). The wild-type strain of *C. elegans* was Bristol N2. Additional *E. coli* strains used in this work were B2W5113 (Wild type, Moco+) and JW0764-2 (Δ*moaA753::kan,* Moco-) (70).

C. elegans mutant and transgenic strains used in this work are listed here. When previously published, sources of strains are referenced. Unless a reference is provided, all strains were generated in this study.

Non-transgenic *C. elegans*:

JT307, *egl-9(sa307)* (44)

GR2254, *moc-1(ok366) X* (33)

GR2260, *cdo-1(mg622) X* (33)

GR2261, *cdo-1(mg622) moc-1(ok366) X* (33)

GR2269, *suox-1(gk738847) X* (33)

CB5602, *vhl-1(ok161) X* (39)

USD414, *rhy-1(ok1402) II; suox-1(gk738847) X*

USD421, *egl-9(sa307) V; suox-1(gk738847) X*

USD422, *vhl-1(ok161) suox-1(gk738847) X*

USD430, *egl-9(sa307) V; cdo-1(mg622) suox-1(gk738847) X*

USD431, *hif-1(ia4) egl-9(sa307) V; suox-1(gk738847) X*

USD432, *rhy-1(ok1402) II; egl-9(sa307) V; suox-1(gk738847) X*

USD433, *cth-2(mg599) II; egl-9(sa307) V; suox-1(gk738847) X*

USD434, *egl-9(sa307) X; cysl-1(ok762) suox-1(gk738847) X*

USD512, *rhy-1(ok1402) II* Outcrossed 4x for this work

USD706*, unc-119(ed3) III; cdo-1(mg622) moc-1(ok366) X*

USD920, *cdo-1(rae273) moc-1(ok366) X*

USD921, *egl-9(sa307) V; cdo-1(rae273) X*

USD922, *rhy-1(ok1402) II; cdo-1(rae273) X*

USD937, *egl-9(rae276) V; suox-1(gk738847) X*

MiniMos transgenic lines:

USD531, *unc-119(ed3) III; raeTi1 [pcdo-1::CDO-1::GFP unc-119(+)]*

USD719, *unc-119(ed3) III; cdo-1(mg622) moc-1(ok366); raeTi14 [pcdo-1::CDO-1(C85Y)::GFP unc-119(+)]*

USD720, *unc-119(ed3) III; raeTi15 [Pcdo-1::GFP unc-119(+)]*

USD730, *rhy-1(ok1402) II; unc-119(ed3) III; raeTi15 [Pcdo-1::GFP unc-119(+)]*

USD733, *unc-119(ed3) III; egl-9(sa307) V; raeTi15 [Pcdo-1::GFP unc-119(+)]*

USD739, *unc-119(ed3) III; cdo-1(mg622) moc-1(ok366) X; raeTi1 [pcdo-1::CDO-1::GFP unc-119(+)]*

USD766, *unc-119(ed3) III; cdo-1(mg622) moc-1(ok366) X; raeTi32 [Pcol-10::CDO-1::GFP unc-119(+)]*

USD767, *unc-119(ed3) III; cdo-1(mg622) moc-1(ok366) X; raeTi33 [Pcol-10::CDO-1::GFP unc-119(+)]*

USD776, *rhy-1(ok1402) II; unc-119(ed3) III; hif-1(ia4) V; raeTi15 [Pcdo-1::GFP unc-119(+)]*

USD777, *unc-119(ed3) III; egl-9(sa307) hif-1(ia4) V; raeTi15 [Pcdo-1::GFP unc-119(+)]*

USD780, *rhy-1(ok1402) II; unc-119(ed3) III; cysl-1(ok762) X; raeTi15 [Pcdo-1::GFP unc-119(+)]*

USD787, *unc-119(ed3) III; egl-9(sa307) V; cysl-1(ok762) X; raeTi15 [Pcdo-1::GFP unc-119(+)]*

USD808, *unc-119(ed3) III; cdo-1(mg622) moc-1(ok366) X; raeTi40 [Pcol-10::CDO-1[C85Y]::GFP unc-119(+)]*

USD810, *unc-119(ed3) III; cdo-1(mg622) moc-1(ok366) X; raeTi41 [Pcol-10::CDO-1[C85Y]::GFP unc-119(+)]*

USD940, *unc-119(ed3) III; vhl-1(ok161) X; raeTi15 [Pcdo-1::GFP unc-119(+)]*

USD1160, *unc-119(ed3) III; cysl-1(ok762) X; raeTi15 [Pcdo-1::GFP unc-119(+)]*

USD1161, *unc-119(ed3) III; hif-1(ia4) V; raeTi15 [Pcdo-1::GFP unc-119(+)]*

EMS-derived strains:

USD659, *unc-119(ed3) III; egl-9(rae213) V; raeTi1 [pcdo-1::CDO-1::GFP unc-119(+)]*

USD674, *unc-119(ed3) III; egl-9(rae227) V; raeTi1 [pcdo-1::CDO-1::GFP unc-119(+)]*

USD655, *rhy-1(rae209) II; unc-119(ed3) III; raeTi1 [pcdo-1::CDO-1::GFP unc-119(+)]*

USD656, *rhy-1(rae210) II; unc-119(ed3) III; raeTi1 [pcdo-1::CDO-1::GFP unc-119(+)]*

USD657, *rhy-1(rae211) II; unc-119(ed3) III; raeTi1 [pcdo-1::CDO-1::GFP unc-119(+)]*

USD658, *rhy-1(rae212) II; unc-119(ed3) III; raeTi1 [pcdo-1::CDO-1::GFP unc-119(+)]*

CRISPR/Cas9-derived strains:

USD914, *cdo-1(rae273) X,* CDO-1::GFP

USD926, *egl-9(rae276) V,* EGL-9[H487A]

USD928, *unc-119(ed3) III; egl-9(rae278) V; raeTi15 [Pcdo-1::GFP unc-119(+)]*

MiniMos transgenesis:

Cloning of original plasmid constructs was performed using isothermal/Gibson assembly (71). All MiniMos constructs were assembled in pNL43, which is derived from pCFJ909, a gift from Erik Jorgensen (Addgene plasmid #44480) (72). Details about plasmid construction are described below. MiniMos transgenic animals were generated using established protocols that rescue the *unc-119(ed3)* Unc phenotype (41).

To generate a construct that expressed CDO-1 under the control of its native promoter, we cloned the wild-type *cdo-1* genomic locus from 1,335 base pairs upstream of the *cdo-1* ATG start codon to (and including) codon 190 encoding the final CDO-1 amino acid prior to the TAA stop codon. This wild-type genomic sequence was fused in frame with a C-terminal GFP and *tbb-2* 3'UTR (376 bp downstream of the *tbb-2* stop codon) in the pNL43 plasmid backbone. This plasmid is called pKW24 (P*cdo-1::CDO-1::GFP*).

To generate pKW44, a construct encoding the active site mutant transgene *Pcdo-1::CDO-1(C85Y)::GFP,* we performed Q5 site-directed mutagenesis on pKW24, following manufacturer's instructions (New England Biolabs). In pKW44, codon 85 was mutated from TGC (cysteine) to TAC (tyrosine).

To generate pKW45 (P*cdo-1::GFP*), the 1,335 base pair *cdo-1* promoter was amplified and fused directly to the GFP coding sequence. Both fragments were derived from pKW24, excluding the *cdo-1* coding sequence and introns.

pKW49 is a construct driving *cdo-1* expression from the hypodermal-specific *col-10* promoter (*Pcol-10::CDO-1::GFP*) (52). The *col-10* promoter (1,126 base pairs upstream of the *col-10* start codon) was

amplified and fused upstream of the *cdo-1* ATG start codon in pKW24, replacing the native *cdo-1* promoter. pKW53 [P*col-10::CDO-1(C85Y)::GFP*] was engineered using the same Q5-site-directed mutagenesis strategy as was described for pKW44. However, this mutagenesis used pKW49 as the template plasmid.

Chemical mutagenesis and whole genome sequencing

To define *C. elegans* gene activities that were necessary for the control of *cdo-1* levels, we carried out a chemical mutagenesis screen for animals that accumulate CDO-1 protein. To visualize CDO-1 levels, we engineered USD531, a transgenic *C. elegans* strain carrying the *raeTi1* [pKW24, *Pcdo-1::CDO-1::GFP*] transgene. USD531 transgenic *C. elegans* were mutagenized with ethyl methanesulfonate (EMS) using established protocols (43). F2 generation animals were manually screened, and mutant isolates were collected that displayed high accumulation of *Pcdo-1::CDO-1::GFP.* We demanded that mutant strains of interest were viable and fertile.

We followed established protocols to identify EMS-induced mutations in our strains of interest (73). Briefly, whole genomic DNA was prepared from *C. elegans* using the Gentra Puregene Tissue Kit (Qiagen) and genomic DNA libraries were prepared using the NEBNext genomic DNA library construction kit (New England Biolabs). DNA libraries were sequenced on an Illumina Hi-Seq and deep sequencing reads were analyzed using standard methods on Galaxy, a web-based platform for computational analyses (74). Briefly, sequencing reads were trimmed and aligned to the WBcel235 *C. elegans* reference genome (75, 76). Variations from the reference genome and the putative impact of those variations were annotated and extracted for analysis (77-79). Here we report the analysis of 6 new mutant strains (USD655, USD656, USD657, USD658, USD659, and USD674). Among these mutant strains, we found 2 unique mutations in *egl-9* (USD659 and USD674) and 4 unique mutations in *rhy-1* (USD655, USD656, USD657, USD658). The allele names and molecular identity of these new *egl-9* and *rhy-1* mutations are specified in Fig. 1C. These genes were prioritized based on the isolation of multiple independent alleles and their established functions in a common pathway, the hypoxia and H_2S-sensing pathway (36-38).

Genome engineering by CRISPR/Cas9

We followed standard protocols to perform CRISPR/Cas9 genome engineering of *cdo-1* and *egl-9* genomic loci in *C. elegans* (80-83). Essential details of the CRISPR/Cas9-generated reagents in this work are described below.

We used homology-directed repair to generate *cdo-1(rae273)* [CDO-1::GFP]. The guide RNA was 5'-gactacagaggatctaagaa-3' (crRNA, IDT). The GFP donor double-stranded DNA (dsDNA) was amplified from pCFJ2249 using primers that contained roughly 40bp of homology to *cdo-1* flanking the desired insertion site (84). The primers used to generate the donor dsDNA were: 5'-gtacggcaagaaagttgactacagaggatctaagaataatagtactagcggtggcagtgg-3' and 5'-agaatcaacacgttattacattgagggatatgttgtttacttgtagagctcgtccattcc-3'. Glycine 189 of CDO-1 was removed by design to eliminate the PAM site and prevent cleavage of the donor dsDNA.

The *egl-9(rae276)* and *egl-9(rae278)* [EGL-9(H487A)] alleles were also generated by homology-directed repair using the same combination of guide RNA and single-stranded oligodeoxynucleotide (ssODN)

donor. The guide RNA was 5'-tgtgaagcatgtagataatc-3' (crRNA, IDT) The ssODN donor was 5'-gcttgccatctatcctggaaatggaactcgttatgtgaaggctgtagacaatccagtaaaagatggaagatgtataaccactatttattactg-3' (Ultramer, IDT). Successful editing resulted in altering the coding sequence of EGL-9 to encode for an alanine rather than the catalytically essential histidine at position 487. We also used synonymous mutations to introduce an AccI restriction site that is helpful for genotyping the *rae276* and *rae278* mutant alleles.

C. elegans growth assays:

To assay developmental rates, *C. elegans* were synchronized at the first stage of larval development. To synchronize animals, embryos were harvested from gravid adult animals via treatment with a bleach and sodium hydroxide solution. Embryos were then incubated overnight in M9 solution causing them to hatch and arrest development at the L1 stage (85). Synchronized L1 animals were cultured on NGM seeded with B2W5113 (Wild type, Moco+) or JW0764-2 (Δ*moaA753::kan,* Moco-) *E. coli.* Animals were cultured for 48 or 72 hours (specified in the appropriate figure legends), and live animals were imaged as described below. Animal length was measured from tip of head to the end of the tail.

To determine qualitative 'health' of various *C. elegans* strains, we assayed the ability of these strains to consume all *E. coli* food provided on an NGM petri dish. For this experiment, dietary *E. coli* was produced via overnight culture in liquid LB in a 37°C shaking incubator. 200μl of this *E. coli* was seeded onto NGM petri dishes and allowed to dry, producing nearly identical lawns and growth environments. Then, 5 L4 animals of a strain of interest were introduced onto these NGM petri dishes seeded with OP50. For each experiment, petri dishes were monitored daily and scored when all *E. coli* was consumed by the population of animals. This assay is beneficial because it integrates many life-history measures (i.e. developmental rate, brood size, embryonic viability, etc.) into a single simple assay that can be scaled and applied to many *C. elegans* strains in parallel.

Cysteine exposure:

To determine the impact of supplemental cysteine on expression of *cdo-1* and animal viability, we exposed various *C. elegans* strains to 0 or 100μM supplemental cysteine. Wild-type and mutant animals carrying the *Pcdo-1::GFP* or CDO-1::GFP transgenes were synchronously grown on NGM media supplemented with *E. coli* OP50 at 20°C until reaching the L4 stage of development. Live L4 animals were then collected from the petri dishes and cultured in liquid M9 media containing 4X concentrated *E. coli* OP50 with or without 100μM supplemental cysteine. These liquid cultures were gently rocked at 20°C overnight. Post exposure, GFP imaging was performed as described in the Microscopy section of the materials and methods. A subset of the assayed animals were also scored for viability after being seeded onto NGM petri dishes. Animals were determined to be alive if they responded to mechanical stimulus.

Microscopy:

Low magnification bright field and fluorescence images (imaging GFP simultaneously in multiple animals) were collected using a Zeiss AxioZoom V16 microscope equipped with a Hamamatsu Orca flash 4.0 digital camera using Zen software (Zeiss). For experiments with supplemental cysteine, low magnification bright field and fluorescence images were collected using a Nikon SMZ25 microscope equipped with a

Hamamatsu Orca flash 4.0 digital camera using NIS-Elements software (Nikon). High magnification differential interference contrast (DIC) and GFP fluorescence images (imaging CDO-1::GFP encoded by *cdo-1(rae273)*) were collected using Zeiss AxioImager Z1 microscope equipped with a Zeiss AxioCam HRc digital camera using Zen software (Zeiss). All images were processed and analyzed using ImageJ software (NIH). All imaging was performed on live animals paralyzed using 20mM sodium azide. For all fluorescence images shown within the same figure panel, images were collected using the same exposure time and processed identically. To quantify GFP expression, the average pixel intensity was determined within a set transverse section immediately anterior to the developing vulva. Background pixel intensity was determined in a set region of interest distinct from the *C. elegans* samples and was subtracted from the sample measurements.

Acknowledgements:

Some *C. elegans* strains were provided by the CGC, which is funded by the NIH Office of Research Infrastructure Programs (P40 OD010440). Research reported in this publication was supported by the National Institute of General Medical Sciences of the National Institutes of Health under award numbers R01 GM044619 (to G.R.) and R35 GM146871 (to K.W.).

Figures:

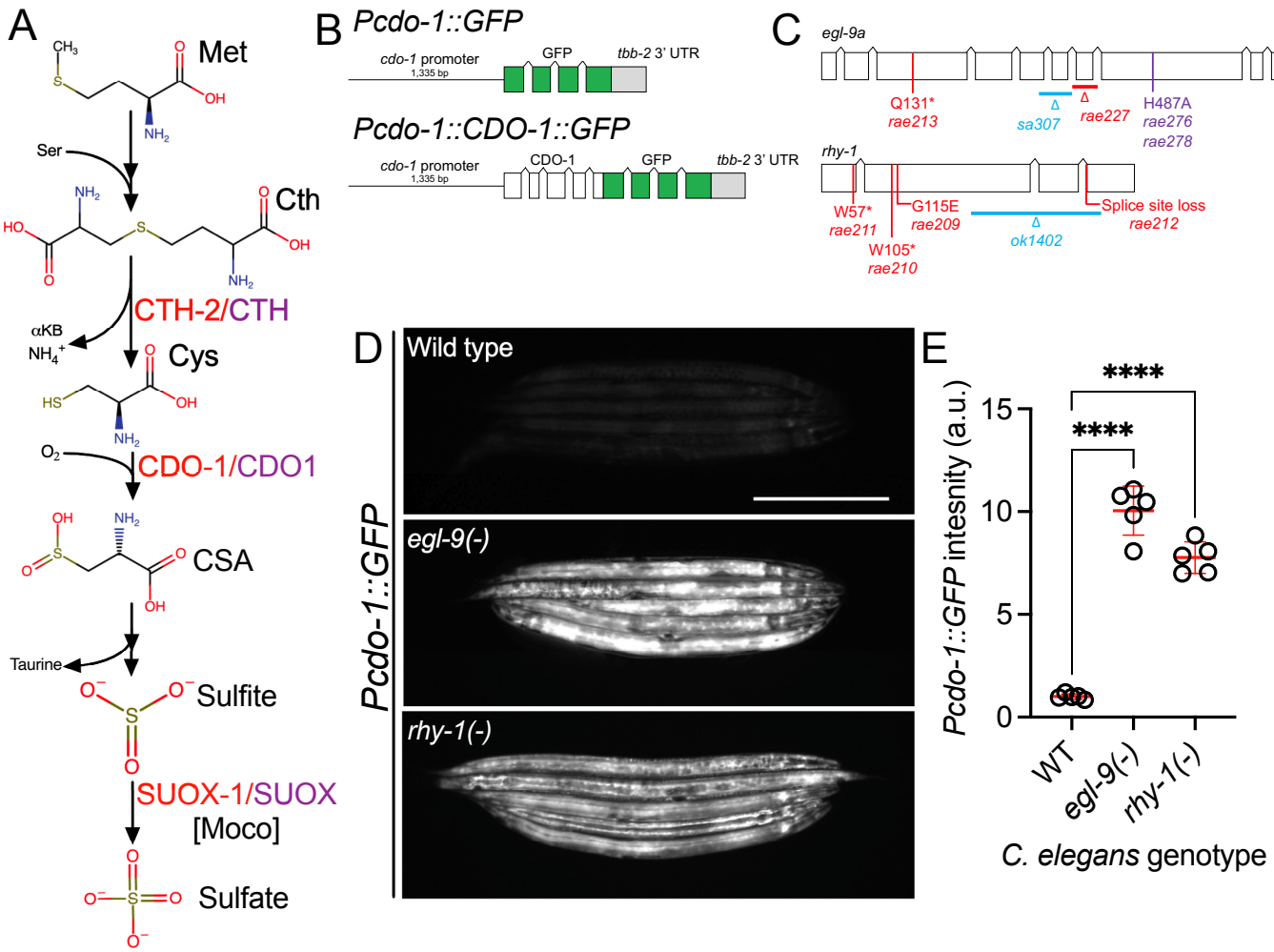

Figure 1: *egl-9* and *rhy-1* inhibit *cdo-1* transcription.

A) Simplified pathway for sulfur amino acid metabolism beginning with methionine. We highlight the roles of cystathionase (CTH-2), cysteine dioxygenase (CDO-1), and the Moco-requiring sulfite oxidase enzyme (SUOX-1). Human homologs are displayed in purple. Abbreviations are as follows: Met (methionine), Ser (serine), Cth (cystathionine), Cys (cysteine), CSA (cysteinesulfinate), and αKB (α-ketobutyrate). B) Models of *Pcdo-1::GFP* (upper) and *Pcdo-1::CDO-1::GFP* (lower) transgenes used in this work are displayed. Boxes indicate exons, connecting lines indicate introns. The *cdo-1* promoter is shown. C) *egl-9a* and *rhy-1* gene structures are displayed. Boxes indicate exons and connecting lines are introns. Colored annotations indicate mutations generated or used in our work. Red; chemically-induced mutations that activated *Pcdo-1::CDO-1::GFP.* Blue; reference null alleles isolated independent of our work. Purple; CRISPR/Cas9-generated mutation that inactivates the prolyl hydroxylase domain of EGL-9. D) Expression of *Pcdo-1::GFP* transgene is displayed from wild-type, *egl-9(sa307),* and *rhy-1(ok1402) C. elegans* animals at the L4 stage of development. Scale bar is 250μm. E) Quantification of GFP expression displayed in Fig. 1D. Individual datapoints are shown (circles) as are the mean and standard deviation (red lines). *n* is 5 individuals per genotype. Data are normalized so that wild-type expression of *Pcdo-1::GFP* is 1 arbitrary unit (a.u.). ****, $p<0.0001$, ordinary one-way ANOVA with Dunnett's post hoc analysis.

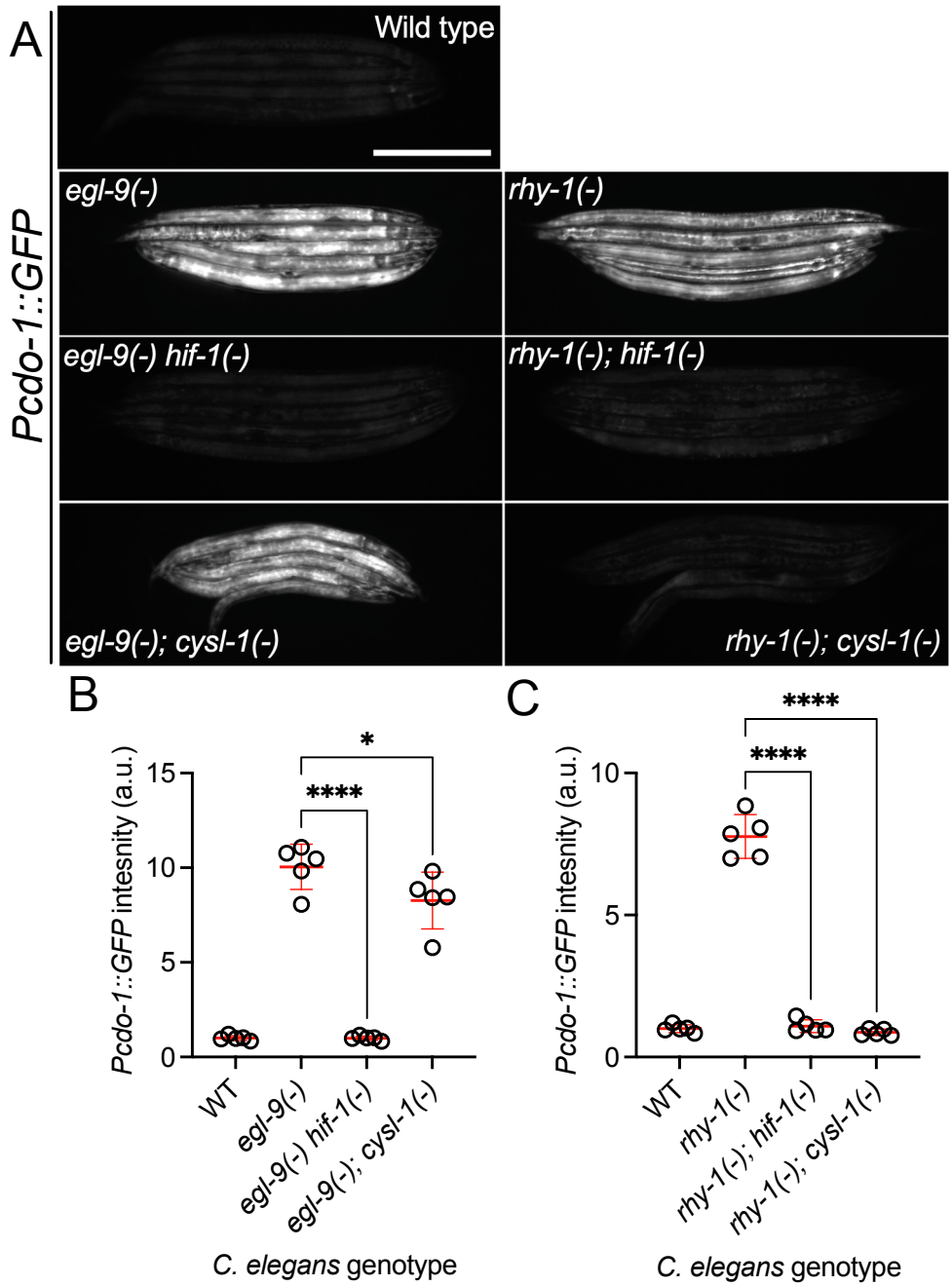

Figure 2: *cdo-1* transcription is activated by *hif-1* downstream of *rhy-1, cysl-1,* and *egl-9.*

A) Expression of the *Pcdo-1::GFP* transgene is displayed for wild-type, *egl-9(sa307), egl-9(sa307) hif-1(ia4)* double mutant, *egl-9(sa307); cysl-1(ok762)* double mutant, *rhy-1(ok1402), rhy-1(ok1402); hif-1(ia4)* double mutant, and *rhy-1(ok1402); cysl-1(ok762)* double mutant *C. elegans* animals at the L4 stage of development. Scale bar is 250μm. B,C) Quantification of the data displayed in Fig. 2A. Individual datapoints are shown (circles) as are the mean and standard deviation (red lines). *n* is 5 individuals per genotype. Data are normalized so that wild-type expression of *Pcdo-1::GFP* is 1 arbitrary unit (a.u.). *, $p<0.05$, ****, $p<0.0001$, ordinary one-way ANOVA with Dunnett's post hoc analysis. Note, wild-type, *egl-9(-),* and *rhy-1(-)* images in panel A and quantification of *Pcdo-1::GFP* in panels B and C are identical to the data presented in Fig. 1D,E. They are re-displayed here to allow for clear comparisons to the double mutant strains of interest.

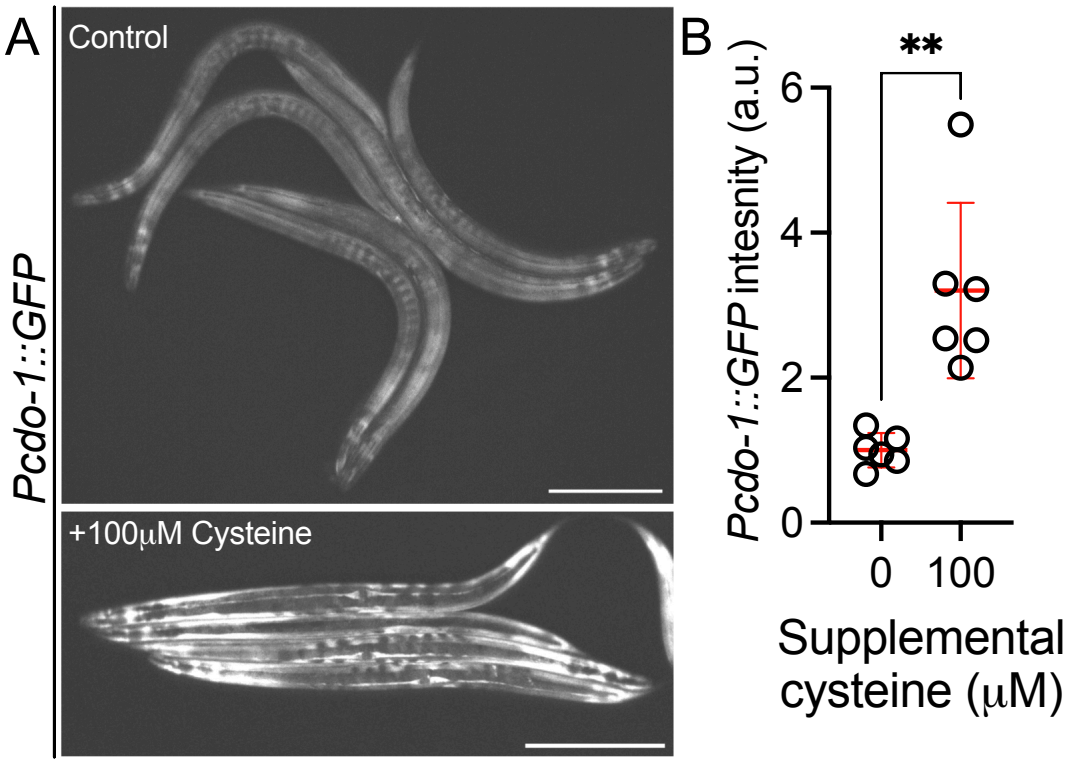

Figure 3: High cysteine activates *cdo-1* transcription.

A) Expression of the *Pcdo-1::GFP* transgene is displayed for wild-type, young-adult *C. elegans* exposed to 100μM supplemental cysteine as well as non-supplemented control animals. Scale bar is 250μm. B) Quantification of the data displayed in Fig. 3A. Individual datapoints are shown (circles) as are the mean and standard deviation (red lines). *n* is 6 individuals per genotype. Data are normalized so that expression of *Pcdo-1::GFP* in wild-type *C. elegans* exposed to 0μM supplemental cysteine is equal to 1 arbitrary unit (a.u.). **, $p<0.001$, Welch's t test.

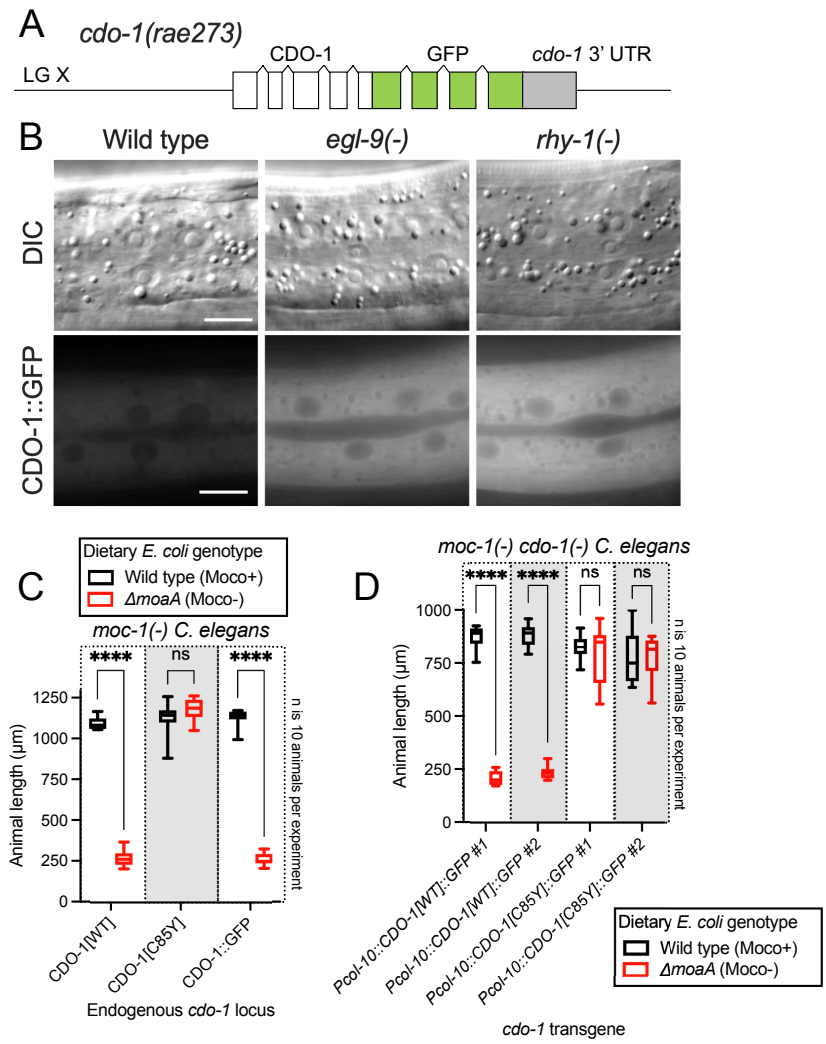

Figure 4: Hypodermal CDO-1 accumulates in the cytoplasm when *egl-9* or *rhy-1* are inactive and is sufficient to promote sulfur amino acid metabolism.

A) Diagram of *cdo-1(rae273),* a CRISPR/Cas9-generated allele where GFP is inserted into endogenous *cdo-1,* creating a C-terminal CDO-1::GFP fusion protein expressed from the native *cdo-1* locus. B) Differential interference contrast (DIC) and fluorescence imaging are shown for wild-type, *egl-9(sa307),* and *rhy-1(ok1402) C. elegans* expressing CDO-1::GFP encoded by *cdo-1(rae273).* Scale bar is 10µm. An anterior segment of the Hyp7 hypodermal cell is displayed. CDO-1::GFP accumulates in the cytoplasm and is excluded from the nuclei. C) *moc-1(ok366), moc-1(ok366) cdo-1(mg622),* and *moc-1(ok366) cdo-1(rae273)* animals were cultured from synchronized L1 larvae for 72 hours on wild-type (black, Moco+) or Δ*moaA* mutant (red, Moco-) *E. coli.* D) *moc-1(ok366) cdo-1(mg622)* double mutant animals expressing *Pcol-10::CDO-1::GFP* or *Pcol-10::CDO-1[C85Y]::GFP* transgenes were cultured for 48 hours on wild-type (black, Moco+) or Δ*moaA* mutant (red, Moco-) *E. coli.* Two independently derived strains were tested for each transgene. For panels C and D, animal lengths were determined for each condition. Box plots display the median, upper, and lower quartiles and whiskers indicate minimum and maximum data points. Sample size (*n*) is 10 individuals for each experiment. ****, $p<0.0001$, multiple unpaired t test with Welch correction. ns indicates no significant difference was identified.

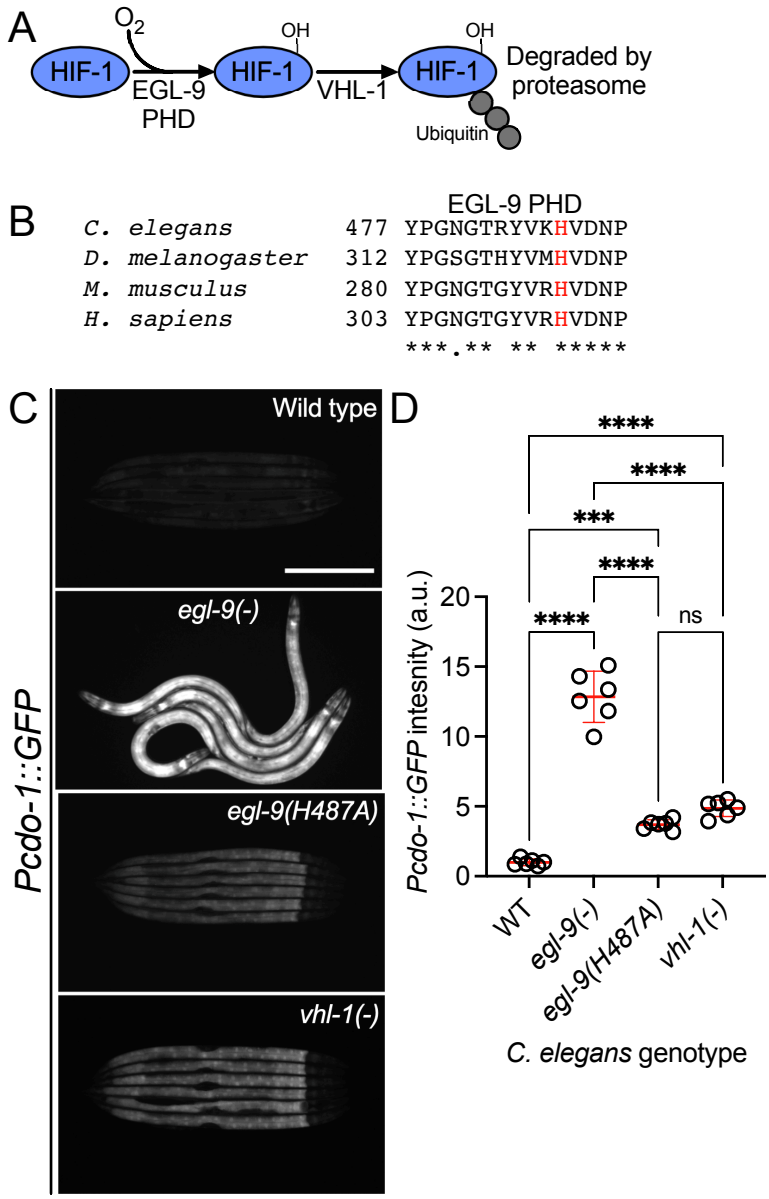

Figure 5: *egl-9* inhibits *cdo-1* transcription in a prolyl-hydroxylase and VHL-1-independent manner. A) The pathway of HIF-1 processing during normoxia is displayed. EGL-9 uses O_2 as a substrate to hydroxylate (-OH) HIF-1 on specific proline residues. Prolyl hydroxylated HIF-1 is bound by VHL-1 which facilitates HIF-1 polyubiquitination and targets HIF-1 for degradation by the proteasome. B) Amino acid alignment of the EGL-9 prolyl hydroxylase domain from *C. elegans, D. melanogaster, M. musculus,* and *H. sapiens.* "*" indicate perfect amino acid conservation while "." indicates weak similarity. Highlighted (red) is the catalytically essential histidine 487 residue in *C. elegans*. Alignment was performed using Clustal Omega (EMBL-EBI). C) Expression of *Pcdo-1::GFP* transgene is displayed for wild-type, *egl-9(sa307, -), vhl-1(ok161),* and *egl-9(rae276,* H487A) *C. elegans* animals at the L4 stage of development. Scale bar is 250μm. D) Quantification of the data displayed in Fig. 5C. Individual datapoints are shown (circles) as are the mean and standard deviation (red lines). *n* is 6 individuals per genotype. Data are normalized so that wild-type expression of *Pcdo-1::GFP* is 1 arbitrary unit (a.u.). ***, $p<0.001$, ****, $p<0.0001$, ordinary one-way ANOVA with Tukey's multiple comparisons test. ns indicates no significant difference was identified.

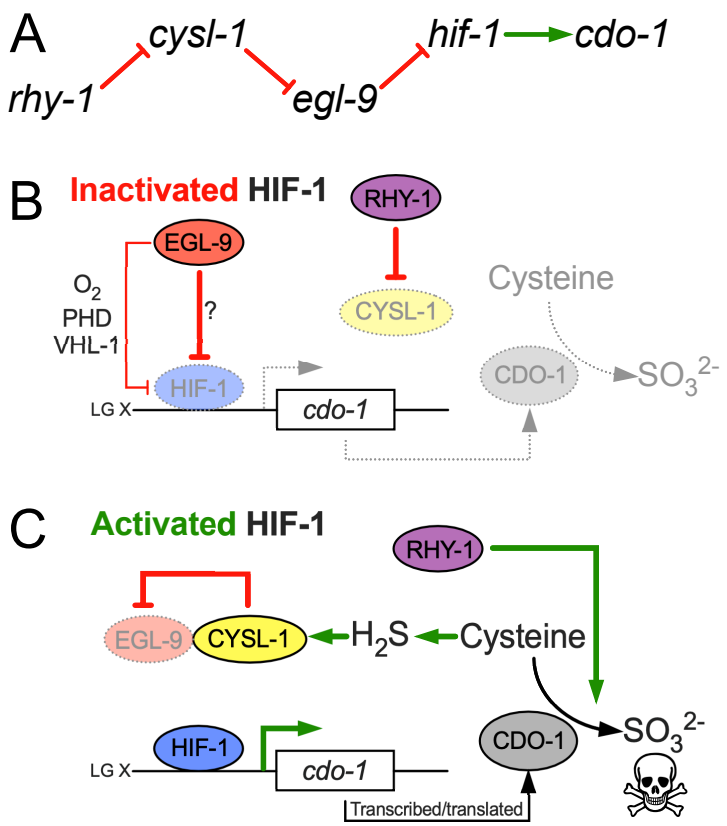

Figure 6: Model for the regulation of cysteine metabolism by HIF-1.

A) Proposed genetic pathway for the regulation of *cdo-1. rhy-1, cysl-1,* and *egl-9* act in a negative-regulatory cascade to control activity of the HIF-1 transcription factor, which activates transcription of *cdo-1.* B) Under basal conditions (inactivated HIF-1), EGL-9 negatively regulates HIF-1 through 2 distinct pathways; one pathway is dependent upon O_2, prolyl hydroxylation (PHD), and VHL-1, while the second acts independently of these canonical factors. Under these conditions *cdo-1* transcription is kept at basal levels and cysteine catabolism is not induced. C) During conditions where HIF-1 is activated (high H_2S), CYSL-1 directly binds and inhibits EGL-9, preventing HIF-1 inactivation. Active HIF-1 binds the *cdo-1* promoter, driving transcription and promoting CDO-1 protein accumulation. High CDO-1 promotes the catabolism of cysteine. HIF-1-induced cysteine catabolism requires the activity of *rhy-1.*

C. elegans strain	Genetic locus 1	Genetic locus 2	Genetic locus 3	Days for population to starve petri dish ± SD (*n*)	Significant difference compared to GR2269 (Adjusted P Value)
N2	Wild type	Wild type	Wild type	5±1 (8)	No test
GR2269	Wild type	*suox-1(gk738847)*	Wild type	8±1 (4)	No test
JT307	*egl-9(sa307)*	Wild type	Wild type	7±1 (5)	No test
USD421	*egl-9(sa307)*	*suox-1(gk738847)*	Wild type	19±5 (11)	0.0003 (***)
USD926	*egl-9(rae276)*	Wild type	Wild type	6±1 (3)	No test
USD937	*egl-9(rae276)*	*suox-1(gk738847)*	Wild type	9±1 (3)	0.93 (ns)
USD512	*rhy-1(ok1402)*	Wild type	Wild type	6±0 (4)	No test
USD414	*rhy-1(ok1402)*	*suox-1(gk738847)*	Wild type	7±0 (4)	0.99 (ns)
CB5602	*vhl-1(ok161)*	Wild type	Wild type	6±0 (4)	No test
USD422	*vhl-1(ok161)*	*suox-1(gk738847)*	Wild type	8±1 (4)	0.99 (ns)
***C. elegans* strain**	**Genetic locus 1**	**Genetic locus 2**	**Genetic locus 3**	**Days for population to starve petri dish ± SD (n)**	**Significant difference compared to USD421 (Adjusted P value)**
USD421	*egl-9(sa307)*	*suox-1(gk738847)*	Wild type	19±5 (11)	No test
USD430	*egl-9(sa307)*	*suox-1(gk738847)*	*cdo-1(mg622)*	7±0 (6)	<0.0001 (****)
USD433	*egl-9(sa307)*	*suox-1(gk738847)*	*cth-2(mg599)*	9±1 (4)	<0.0001 (****)
USD432	*egl-9(sa307)*	*suox-1(gk738847)*	*rhy-1(ok1402)*	7±1 (4)	<0.0001 (****)
USD434	*egl-9(sa307)*	*suox-1(gk738847)*	*cysl-1(ok762)*	16±1 (9)	0.1 (ns)
USD431	*egl-9(sa307)*	*suox-1(gk738847)*	*hif-1(ia4)*	9±1 (6)	<0.0001 (****)

Table 1: Growth of *C. elegans* strains on standard laboratory conditions.

C. elegans strains and their corresponding mutations are displayed. For each strain, 5 L4-stage animals were seeded onto standard NGM petri dishes seeded with a monoculture of *E. coli* OP50. Petri dishes were monitored until the animals (and their progeny) depleted the lawn of *E. coli*. This was recorded as “days for population to starve petri dish”. The average of these experiments is displayed for each *C. elegans* strain as is the standard deviation (SD) and the number of biological replicates (*n*). Significant differences in population growth were determined by appropriate comparisons to either *suox-1(gk738847)* (GR2269) or *egl-9(sa307); suox-1(gk738847)* (USD421) using an ordinary one-way ANOVA with Dunnett’s post hoc analysis. No test indicates a statistical comparison was not made. Note, the data for USD421 are displayed twice in the table to allow for ease of comparison.

Supplemental Figures:

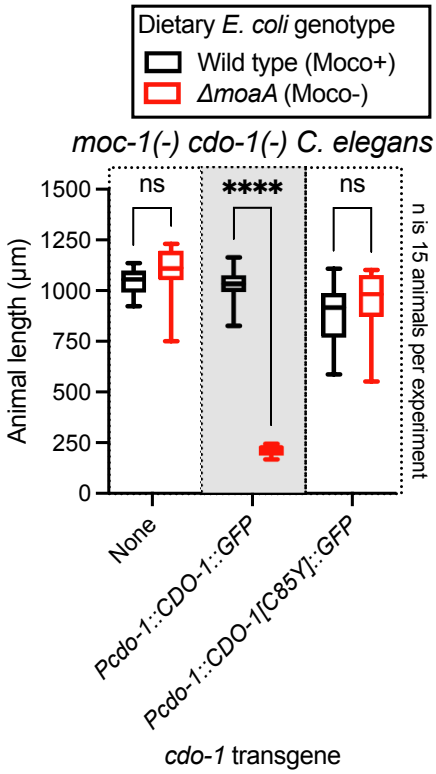

Figure S1: The *Pcdo-1::CDO-1::GFP* transgene encodes a functional cysteine dioxygenase enzyme. *moc-1(ok366) cdo-1(mg622)* double mutant animals expressing *Pcdo-1::CDO-1::GFP* or *Pcdo-1::CDO-1[C85Y]::GFP* transgenes were cultured for 72 hours on wild-type (black, Moco+) or Δ*moaA* mutant (red, Moco-) *E. coli.* Animal lengths were determined for each condition. Box plots display the median, upper, and lower quartiles and whiskers indicate minimum and maximum data points. Sample size (*n*) is displayed for each experiment. ****, $p<0.0001$, multiple unpaired t test with Welch correction. ns indicates no significant difference was identified.

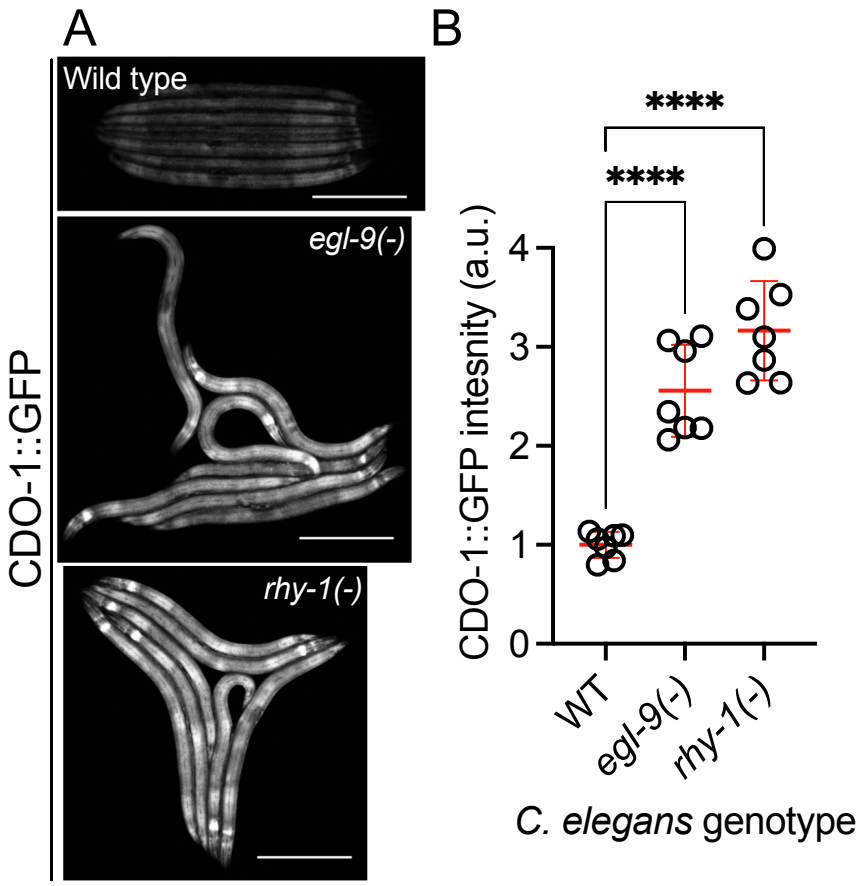

Figure S2: A functional CDO-1::GFP fusion protein is induced by loss of *egl-9* or *rhy-1.*

A) Expression of CDO-1::GFP from the *cdo-1(rae273)* allele is displayed for wild-type, *egl-9(sa307),* and *rhy-1(ok1402)* animals at the L4 stage of development. Scale bar is 250μm. B) Quantification of CDO-1::GFP expression displayed in Fig. S2A. Individual datapoints are shown (circles) as are the mean and standard deviation (red lines). *n* is 7 individuals per genotype. Data are normalized so that wild-type expression of CDO-1::GFP is 1 arbitrary unit (a.u.). ****, $p<0.0001$, ordinary one-way ANOVA with Dunnett's post hoc analysis.

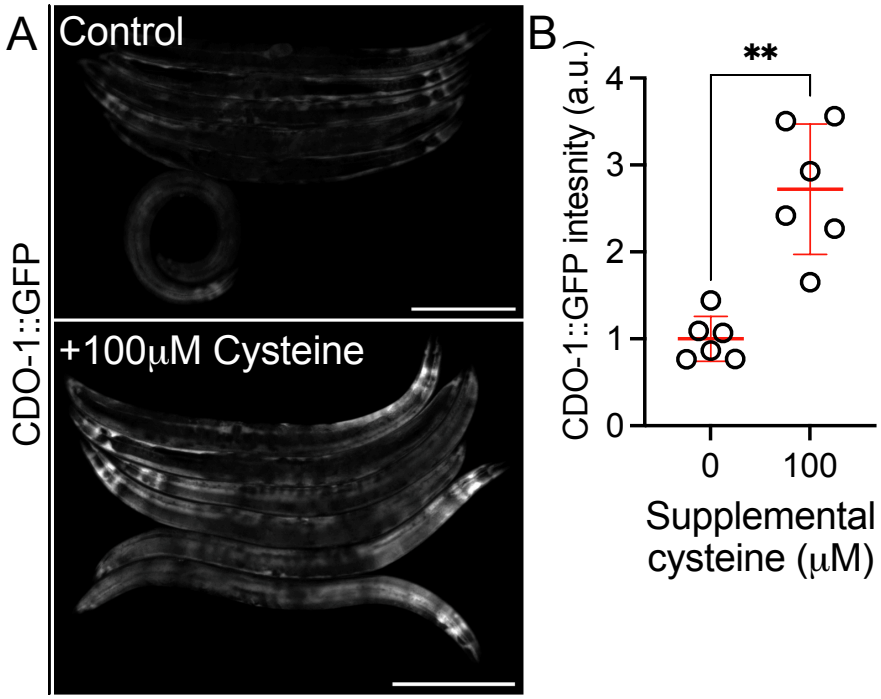

Figure S3: CDO-1::GFP encoded by *cdo-1(rae273)* is induced by supplemental cysteine.

A) Expression of CDO-1::GFP from the *cdo-1(rae273)* allele is displayed for wild type young adult animals exposed to 0 or 100μM supplemental cysteine. Scale bar is 250μm. B) Quantification of CDO-1::GFP expression displayed in Fig. S3A. Individual datapoints are shown (circles) as are the mean and standard deviation (red lines). *n* is 6 individuals per genotype. Data are normalized so that wild-type expression of CDO-1::GFP exposed to 0μM supplemental cysteine is 1 arbitrary unit (a.u.). **, $p<0.001$, Welch's t test.

References:

1. G. Wu, Y. Z. Fang, S. Yang, J. R. Lupton, N. D. Turner, Glutathione metabolism and its implications for health. *J Nutr* **134**, 489-492 (2004).
2. S. Singh, R. Banerjee, PLP-dependent H(2)S biogenesis. *Biochim Biophys Acta* **1814**, 1518-1527 (2011).
3. L. Zheng, R. H. White, V. L. Cash, R. F. Jack, D. R. Dean, Cysteine desulfurase activity indicates a role for NIFS in metallocluster biosynthesis. *Proc Natl Acad Sci U S A* **90**, 2754-2758 (1993).
4. R. Noiva, Enzymatic catalysis of disulfide formation. *Protein Expr Purif* **5**, 1-13 (1994).
5. S. Raina, D. Missiakas, Making and breaking disulfide bonds. *Annu Rev Microbiol* **51**, 179-202 (1997).
6. A. Rietsch, J. Beckwith, The genetics of disulfide bond metabolism. *Annu Rev Genet* **32**, 163-184 (1998).
7. N. M. Giles *et al.*, Metal and redox modulation of cysteine protein function. *Chem Biol* **10**, 677-693 (2003).
8. J. A. Tainer, V. A. Roberts, E. D. Getzoff, Metal-binding sites in proteins. *Curr Opin Biotechnol* **2**, 582-591 (1991).
9. J. Miller, A. D. McLachlan, A. Klug, Repetitive zinc-binding domains in the protein transcription factor IIIA from Xenopus oocytes. *Embo j* **4**, 1609-1614 (1985).
10. C. E. Hughes *et al.*, Cysteine Toxicity Drives Age-Related Mitochondrial Decline by Altering Iron Homeostasis. *Cell* **180**, 296-310.e218 (2020).
11. J. W. Olney, C. Zorumski, M. T. Price, J. Labruyere, L-cysteine, a bicarbonate-sensitive endogenous excitotoxin. *Science* **248**, 596-599 (1990).
12. C. L. Evans, The toxicity of hydrogen sulphide and other sulphides. *Q J Exp Physiol Cogn Med Sci* **52**, 231-248 (1967).

13. D. H. Truong, M. A. Eghbal, W. Hindmarsh, S. H. Roth, P. J. O'Brien, Molecular mechanisms of hydrogen sulfide toxicity. *Drug Metab Rev* **38**, 733-744 (2006).
14. M. H. Stipanuk, Sulfur amino acid metabolism: pathways for production and removal of homocysteine and cysteine. *Annu Rev Nutr* **24**, 539-577 (2004).
15. D. L. Bella, Y. H. Kwon, M. H. Stipanuk, Variations in dietary protein but not in dietary fat plus cellulose or carbohydrate levels affect cysteine metabolism in rat isolated hepatocytes. *J Nutr* **126**, 2179-2187 (1996).
16. M. H. Stipanuk, I. Ueki, Dealing with methionine/homocysteine sulfur: cysteine metabolism to taurine and inorganic sulfur. *J Inherit Metab Dis* **34**, 17-32 (2011).
17. J. E. Dominy, Jr., L. L. Hirschberger, R. M. Coloso, M. H. Stipanuk, In vivo regulation of cysteine dioxygenase via the ubiquitin-26S proteasome system. *Adv Exp Med Biol* **583**, 37-47 (2006).
18. J. E. Dominy, Jr., L. L. Hirschberger, R. M. Coloso, M. H. Stipanuk, Regulation of cysteine dioxygenase degradation is mediated by intracellular cysteine levels and the ubiquitin-26 S proteasome system in the living rat. *Biochem J* **394**, 267-273 (2006).
19. M. H. Stipanuk, L. L. Hirschberger, M. P. Londono, C. L. Cresenzi, A. F. Yu, The ubiquitin-proteasome system is responsible for cysteine-responsive regulation of cysteine dioxygenase concentration in liver. *Am J Physiol Endocrinol Metab* **286**, E439-448 (2004).
20. J. I. Lee, M. Londono, L. L. Hirschberger, M. H. Stipanuk, Regulation of cysteine dioxygenase and gamma-glutamylcysteine synthetase is associated with hepatic cysteine level. *J Nutr Biochem* **15**, 112-122 (2004).
21. Y. H. Kwon, M. H. Stipanuk, Cysteine regulates expression of cysteine dioxygenase and gamma-glutamylcysteine synthetase in cultured rat hepatocytes. *Am J Physiol Endocrinol Metab* **280**, E804-815 (2001).
22. K. Kojima *et al.*, Cysteine dioxygenase type 1 (CDO1) gene promoter methylation during the adenoma-carcinoma sequence in colorectal cancer. *PLoS One* **13**, e0194785 (2018).
23. K. Yamashita, K. Hosoda, N. Nishizawa, H. Katoh, M. Watanabe, Epigenetic biomarkers of promoter DNA methylation in the new era of cancer treatment. *Cancer Sci* **109**, 3695-3706 (2018).
24. M. Brait *et al.*, Cysteine dioxygenase 1 is a tumor suppressor gene silenced by promoter methylation in multiple human cancers. *PLoS One* **7**, e44951 (2012).
25. Y. P. Kang *et al.*, Cysteine dioxygenase 1 is a metabolic liability for non-small cell lung cancer. *Elife* **8** (2019).
26. J. Jeschke *et al.*, Frequent inactivation of cysteine dioxygenase type 1 contributes to survival of breast cancer cells and resistance to anthracyclines. *Clin Cancer Res* **19**, 3201-3211 (2013).
27. S. Hao *et al.*, Cysteine Dioxygenase 1 Mediates Erastin-Induced Ferroptosis in Human Gastric Cancer Cells. *Neoplasia* **19**, 1022-1032 (2017).
28. G. Ma *et al.*, Cysteine dioxygenase 1 attenuates the proliferation via inducing oxidative stress and integrated stress response in gastric cancer cells. *Cell Death Discov* **8**, 493 (2022).
29. M. Duran *et al.*, Combined deficiency of xanthine oxidase and sulphite oxidase: a defect of molybdenum metabolism or transport? *J Inherit Metab Dis* **1**, 175-178 (1978).
30. S. H. Mudd, F. Irreverre, L. Laster, Sulfite oxidase deficiency in man: demonstration of the enzymatic defect. *Science* **156**, 1599-1602 (1967).
31. G. Schwarz, R. R. Mendel, M. W. Ribbe, Molybdenum cofactors, enzymes and pathways. *Nature* **460**, 839-847 (2009).
32. Y. Zhang, V. N. Gladyshev, Molybdoproteomes and evolution of molybdenum utilization. *J Mol Biol* **379**, 881-899 (2008).
33. K. Warnhoff, G. Ruvkun, Molybdenum cofactor transfer from bacteria to nematode mediates sulfite detoxification. *Nat Chem Biol* **15**, 480-488 (2019).
34. K. Warnhoff, T. W. Hercher, R. R. Mendel, G. Ruvkun, Protein-bound molybdenum cofactor is bioavailable and rescues molybdenum cofactor-deficient C. elegans. *Genes Dev* **35**, 212-217 (2021).
35. J. Snoozy, P. C. Breen, G. Ruvkun, K. Warnhoff, moc-6/MOCS2A is necessary for molybdenum cofactor synthesis in C. elegans. *MicroPubl Biol* **2022** (2022).
36. C. Shen, Z. Shao, J. A. Powell-Coffman, The Caenorhabditis elegans rhy-1 gene inhibits HIF-1 hypoxia-inducible factor activity in a negative feedback loop that does not include vhl-1. *Genetics* **174**, 1205-1214 (2006).

37. M. W. Budde, M. B. Roth, The response of Caenorhabditis elegans to hydrogen sulfide and hydrogen cyanide. *Genetics* **189**, 521-532 (2011).
38. D. K. Ma, R. Vozdek, N. Bhatla, H. R. Horvitz, CYSL-1 interacts with the O2-sensing hydroxylase EGL-9 to promote H2S-modulated hypoxia-induced behavioral plasticity in C. elegans. *Neuron* **73**, 925-940 (2012).
39. A. C. Epstein *et al.*, C. elegans EGL-9 and mammalian homologs define a family of dioxygenases that regulate HIF by prolyl hydroxylation. *Cell* **107**, 43-54 (2001).
40. M. Ivan *et al.*, HIFalpha targeted for VHL-mediated destruction by proline hydroxylation: implications for O2 sensing. *Science* **292**, 464-468 (2001).
41. C. Frøkjær-Jensen *et al.*, Random and targeted transgene insertion in Caenorhabditis elegans using a modified Mos1 transposon. *Nat Methods* **11**, 529-534 (2014).
42. J. G. McCoy *et al.*, Structure and mechanism of mouse cysteine dioxygenase. *Proc Natl Acad Sci U S A* **103**, 3084-3089 (2006).
43. S. Brenner, The genetics of Caenorhabditis elegans. *Genetics* **77**, 71-94 (1974).
44. C. Darby, C. L. Cosma, J. H. Thomas, C. Manoil, Lethal paralysis of Caenorhabditis elegans by Pseudomonas aeruginosa. *Proc Natl Acad Sci U S A* **96**, 15202-15207 (1999).
45. B. Wang *et al.*, Co-opted genes of algal origin protect C. elegans against cyanogenic toxins. *Curr Biol* **32**, 4941-4948.e4943 (2022).
46. S. Salceda, J. Caro, Hypoxia-inducible factor 1alpha (HIF-1alpha) protein is rapidly degraded by the ubiquitin-proteasome system under normoxic conditions. Its stabilization by hypoxia depends on redox-induced changes. *J Biol Chem* **272**, 22642-22647 (1997).
47. L. E. Huang, J. Gu, M. Schau, H. F. Bunn, Regulation of hypoxia-inducible factor 1alpha is mediated by an O2-dependent degradation domain via the ubiquitin-proteasome pathway. *Proc Natl Acad Sci U S A* **95**, 7987-7992 (1998).
48. C. H. Sutter, E. Laughner, G. L. Semenza, Hypoxia-inducible factor 1alpha protein expression is controlled by oxygen-regulated ubiquitination that is disrupted by deletions and missense mutations. *Proc Natl Acad Sci U S A* **97**, 4748-4753 (2000).
49. C. L. Pender, H. R. Horvitz, Hypoxia-inducible factor cell non-autonomously regulates C. elegans stress responses and behavior via a nuclear receptor. *Elife* **7** (2018).
50. M. M. Kudron *et al.*, The ModERN Resource: Genome-Wide Binding Profiles for Hundreds of Drosophila and Caenorhabditis elegans Transcription Factors. *Genetics* **208**, 937-949 (2018).
51. W. G. Kaelin, Jr., P. J. Ratcliffe, Oxygen sensing by metazoans: the central role of the HIF hydroxylase pathway. *Mol Cell* **30**, 393-402 (2008).
52. Y. Hong, R. C. Lee, V. Ambros, Structure and function analysis of LIN-14, a temporal regulator of postembryonic developmental events in Caenorhabditis elegans. *Mol Cell Biol* **20**, 2285-2295 (2000).
53. K. D. Oliphant, R. R. Fettig, J. Snoozy, R. R. Mendel, K. Warnhoff, Obtaining the necessary molybdenum cofactor for sulfite oxidase activity in the nematode Caenorhabditis elegans surprisingly involves a dietary source. *J Biol Chem* **299**, 102736 (2023).
54. J. W. Horsman, F. I. Heinis, D. L. Miller, A Novel Mechanism To Prevent H(2)S Toxicity in Caenorhabditis elegans. *Genetics* **213**, 481-490 (2019).
55. Y. Pan *et al.*, Multiple factors affecting cellular redox status and energy metabolism modulate hypoxia-inducible factor prolyl hydroxylase activity in vivo and in vitro. *Mol Cell Biol* **27**, 912-925 (2007).
56. Z. Shao, Y. Zhang, J. A. Powell-Coffman, Two distinct roles for EGL-9 in the regulation of HIF-1-mediated gene expression in Caenorhabditis elegans. *Genetics* **183**, 821-829 (2009).
57. G. L. Semenza, G. L. Wang, A nuclear factor induced by hypoxia via de novo protein synthesis binds to the human erythropoietin gene enhancer at a site required for transcriptional activation. *Mol Cell Biol* **12**, 5447-5454 (1992).
58. N. Bashan, E. Burdett, H. S. Hundal, A. Klip, Regulation of glucose transport and GLUT1 glucose transporter expression by O2 in muscle cells in culture. *Am J Physiol* **262**, C682-690 (1992).
59. J. D. Loike *et al.*, Hypoxia induces glucose transporter expression in endothelial cells. *Am J Physiol* **263**, C326-333 (1992).
60. J. D. Firth, B. L. Ebert, C. W. Pugh, P. J. Ratcliffe, Oxygen-regulated control elements in the phosphoglycerate kinase 1 and lactate dehydrogenase A genes: similarities with the erythropoietin 3' enhancer. *Proc Natl Acad Sci U S A* **91**, 6496-6500 (1994).

61. J. M. Gray *et al.*, Oxygen sensation and social feeding mediated by a C. elegans guanylate cyclase homologue. *Nature* **430**, 317-322 (2004).
62. M. W. Budde, M. B. Roth, Hydrogen sulfide increases hypoxia-inducible factor-1 activity independently of von Hippel-Lindau tumor suppressor-1 in C. elegans. *Mol Biol Cell* **21**, 212-217 (2010).
63. D. L. Miller, M. W. Budde, M. B. Roth, HIF-1 and SKN-1 coordinate the transcriptional response to hydrogen sulfide in Caenorhabditis elegans. *PLoS One* **6**, e25476 (2011).
64. C. Shen, D. Nettleton, M. Jiang, S. K. Kim, J. A. Powell-Coffman, Roles of the HIF-1 hypoxia-inducible factor during hypoxia response in Caenorhabditis elegans. *J Biol Chem* **280**, 20580-20588 (2005).
65. H. Jurkowska *et al.*, Primary hepatocytes from mice lacking cysteine dioxygenase show increased cysteine concentrations and higher rates of metabolism of cysteine to hydrogen sulfide and thiosulfate. *Amino Acids* **46**, 1353-1365 (2014).
66. N. O. Burton *et al.*, Intergenerational adaptations to stress are evolutionarily conserved, stress-specific, and have deleterious trade-offs. *Elife* **10** (2021).
67. G. M. Gibbs, K. Roelants, M. K. O'Bryan, The CAP superfamily: cysteine-rich secretory proteins, antigen 5, and pathogenesis-related 1 proteins--roles in reproduction, cancer, and immune defense. *Endocr Rev* **29**, 865-897 (2008).
68. A. R. Frand, J. W. Cuozzo, C. A. Kaiser, Pathways for protein disulphide bond formation. *Trends Cell Biol* **10**, 203-210 (2000).
69. N. Mizuki, M. Kasahara, Mouse submandibular glands express an androgen-regulated transcript encoding an acidic epididymal glycoprotein-like molecule. *Mol Cell Endocrinol* **89**, 25-32 (1992).
70. T. Baba *et al.*, Construction of Escherichia coli K-12 in-frame, single-gene knockout mutants: the Keio collection. *Mol Syst Biol* **2**, 2006.0008 (2006).
71. D. G. Gibson *et al.*, Enzymatic assembly of DNA molecules up to several hundred kilobases. *Nat Methods* **6**, 343-345 (2009).
72. N. J. Lehrbach, G. Ruvkun, Proteasome dysfunction triggers activation of SKN-1A/Nrf1 by the aspartic protease DDI-1. *Elife* **5** (2016).
73. N. J. Lehrbach, F. Ji, R. Sadreyev, Next-Generation Sequencing for Identification of EMS-Induced Mutations in Caenorhabditis elegans. *Curr Protoc Mol Biol* **117**, 7.29.21-27.29.12 (2017).
74. G. Community, The Galaxy platform for accessible, reproducible and collaborative biomedical analyses: 2022 update. *Nucleic Acids Res* **50**, W345-351 (2022).
75. A. M. Bolger, M. Lohse, B. Usadel, Trimmomatic: a flexible trimmer for Illumina sequence data. *Bioinformatics* **30**, 2114-2120 (2014).
76. H. Li, R. Durbin, Fast and accurate long-read alignment with Burrows-Wheeler transform. *Bioinformatics* **26**, 589-595 (2010).
77. A. Wilm *et al.*, LoFreq: a sequence-quality aware, ultra-sensitive variant caller for uncovering cell-population heterogeneity from high-throughput sequencing datasets. *Nucleic Acids Res* **40**, 11189-11201 (2012).
78. P. Cingolani *et al.*, Using Drosophila melanogaster as a Model for Genotoxic Chemical Mutational Studies with a New Program, SnpSift. *Front Genet* **3**, 35 (2012).
79. P. Cingolani *et al.*, A program for annotating and predicting the effects of single nucleotide polymorphisms, SnpEff: SNPs in the genome of Drosophila melanogaster strain w1118; iso-2; iso-3. *Fly (Austin)* **6**, 80-92 (2012).
80. K. S. Ghanta, C. C. Mello, Melting dsDNA Donor Molecules Greatly Improves Precision Genome Editing in Caenorhabditis elegans. *Genetics* **216**, 643-650 (2020).
81. J. A. Arribere *et al.*, Efficient marker-free recovery of custom genetic modifications with CRISPR/Cas9 in Caenorhabditis elegans. *Genetics* **198**, 837-846 (2014).
82. A. Paix, A. Folkmann, G. Seydoux, Precision genome editing using CRISPR-Cas9 and linear repair templates in C. elegans. *Methods* **121-122**, 86-93 (2017).
83. G. A. Dokshin, K. S. Ghanta, K. M. Piscopo, C. C. Mello, Robust Genome Editing with Short Single-Stranded and Long, Partially Single-Stranded DNA Donors in Caenorhabditis elegans. *Genetics* **210**, 781-787 (2018).
84. M. D. Aljohani, S. El Mouridi, M. Priyadarshini, A. M. Vargas-Velazquez, C. Frøkjær-Jensen, Engineering rules that minimize germline silencing of transgenes in simple extrachromosomal arrays in C. elegans. *Nat Commun* **11**, 6300 (2020).
85. T. Stiernagle, Maintenance of C. elegans. *WormBook* 10.1895/wormbook.1.101.1, 1-11 (2006).